Commun. Comput. Phys.
doi: 10.4208/cicp.scpde14.39s

Vol. **19**, No. 5, pp. 1473-1502
May 2016

On Fully Decoupled, Convergent Schemes for Diffuse Interface Models for Two-Phase Flow with General Mass Densities

Günther Grün[1,*], Francisco Guillén-González[2] and Stefan Metzger[1]

[1] *Friedrich-Alexander-Universität Erlangen-Nürnberg, Department Mathematik, Cauerstr. 11, 91058 Erlangen, Germany.*
[2] *Universidad Sevilla, Dpto. Ecuaciones Diferenciales y Análisis Numérico, Instituto de Matemáticas, Aptdo. 1160, 41080, Sevilla, Spain.*

Received 6 March 2015; Accepted 7 December 2015

Abstract. In the first part, we study the convergence of discrete solutions to splitting schemes for two-phase flow with different mass densities suggested in [Guillen-Gonzalez, Tierra, J.Comput.Math. (6)2014]. They have been formulated for the diffuse interface model in [Abels, Garcke, Grün, M3AS, 2012, DOI:10.1142/S0218202511500138] which is consistent with thermodynamics. Our technique covers various discretization methods for phase-field energies, ranging from convex-concave splitting to difference quotient approaches for the double-well potential. In the second part of the paper, numerical experiments are presented in two space dimensions to identify discretizations of Cahn-Hilliard energies which are φ-stable and which do not reduce the acceleration of falling droplets. Finally, 3d simulations in axial symmetric geometries are shown to underline even more the full practicality of the approach.

AMS subject classifications: 35Q35, 65M60, 65M22, 65M12, 76D05, 76T10

Key words: Two-phase flow, Cahn-Hilliard equation, diffuse interface model, convergence of finite-element schemes, numerical simulation.

1 Introduction

In this paper, we are concerned with aspects of numerical analysis and practical computation related to the diffuse interface model for two-phase flow of incompressible, viscous

*Corresponding author. *Email addresses:* gruen@am.uni-erlangen.de (G. Grün), guillen@us.es (F. Guillén-González), stefan.metzger@fau.de (S. Metzger)

 ©2016 Global-Science Press

https://doi.org/10.4208/cicp.scpde14.39s Published online by Cambridge University Press

fluids with different mass densities proposed in [1]. It reads as follows.

$$\bar{\rho}(\varphi)\partial_t \mathbf{v} + \left(\left(\bar{\rho}(\varphi)\mathbf{v} + \frac{\partial\bar{\rho}(\varphi)}{\partial\varphi}\mathbf{j}\right)\cdot\nabla\right)\mathbf{v} - \nabla\cdot(2\eta(\varphi)\mathbf{D}\mathbf{v}) + \nabla p = \mu\nabla\varphi + \mathbf{k}_{\text{grav}}, \tag{1.1a}$$

$$\partial_t\varphi + \mathbf{v}\cdot\nabla\varphi - \nabla\cdot(M(\varphi)\nabla\mu) = 0, \tag{1.1b}$$

$$\mu = \sigma\left(-\varepsilon\Delta\varphi + \tfrac{1}{\varepsilon}F'(\varphi)\right), \tag{1.1c}$$

$$\nabla\cdot\mathbf{v} = 0 \quad \text{in } \Omega\times(0,T). \tag{1.1d}$$

Since we wish to take contact angle hysteresis into account, too, the following boundary conditions are chosen.

$$\sigma\frac{\partial\varphi}{\partial\mathbf{n}} = -\gamma_{LS}' - \alpha\partial_t\varphi \qquad \text{on } \partial\Omega\times(0,T), \tag{1.2a}$$

$$\frac{\partial}{\partial\mathbf{n}}\mu \equiv 0 \qquad \text{on } \partial\Omega\times(0,T), \tag{1.2b}$$

$$\mathbf{v} \equiv 0 \qquad \text{on } \partial\Omega\times(0,T). \tag{1.2c}$$

Here, $\gamma_{LS}(\phi)$ interpolates between the liquid-solid interfacial energies in the pure phases, and $\alpha \geq 0$ is the coefficient related to energy dissipation caused by contact line motion. The parameter σ is the surface tension coefficient, which is assumed to be $\sigma = 1$ in this paper. Note that this approach is inspired by the ideas of [22] where the relationship to contact angle hysteresis is explained. In particular, if $\gamma_{LS} \equiv const.$ and $\alpha \equiv 0$, the system prefers a contact angle θ of 90 degrees, as (1.2a) is a phase-field approximation of Young's law $\cos\theta = (\gamma_{LS}(-1) - \gamma_{LS}(1))/\sigma$, see [22]. Note that system (1.1) couples a hydrodynamic momentum equation with a Cahn-Hilliard type phase-field equation. F is a double-well potential with minima in ± 1 – representing the pure phases $\varphi \equiv \pm 1$. The term μ stands for the so called chemical potential, and the order parameter φ stands for the difference of the volume fractions $u_2 - u_1$ where $u_i(x,t) := \rho_i(x,t)/\tilde{\rho}_i$ with $\tilde{\rho}_i$ the specific (constant) density of fluid i in a unmixed setting. The parameter ε controls the width of the interface region. For the ease of notation we set $\varepsilon = 1$. Denoting the individual velocities by $\mathbf{v}_i$, $i = 1,2$, we write $\mathbf{v} := u_1\mathbf{v}_1 + u_2\mathbf{v}_2$ for the volume averaged velocity. Assuming $\tilde{\rho}_2 \geq \tilde{\rho}_1$, the density of the total mass $\bar{\rho}(\varphi)$ is given by

$$\bar{\rho}(\varphi) = \frac{\tilde{\rho}_2 + \tilde{\rho}_1}{2} + \frac{\tilde{\rho}_2 - \tilde{\rho}_1}{2}\varphi, \tag{1.3}$$

and $\mathbf{D}\mathbf{v}$ denotes the symmetrized gradient. The term $\mathbf{k}_{\text{grav}}$ stands for the density of external volume forces. Finally, the flux $\mathbf{j}$ is defined by $\mathbf{j} := -M(\varphi)\nabla\mu$ where $M(\varphi)$ is the mobility.

It is straightforward to show that the physical energy[†]

$$\overline{\mathcal{E}}(\mathbf{v},\varphi) := \frac{1}{2}\int_\Omega \bar{\rho}(\varphi)|\mathbf{v}|^2 + \frac{\varepsilon}{2}\int_\Omega |\nabla\varphi|^2 + \frac{1}{\varepsilon}\int_\Omega F(\varphi) + \int_{\partial\Omega}\gamma_{LS}(\varphi) \tag{1.4}$$

[†]Note that later in the paper, we will consider regularizations $\rho(\cdot)$ of $\bar{\rho}(\cdot)$. Consistently, we will denote the corresponding energy by $\mathcal{E}(\mathbf{v},\varphi)$.

https://doi.org/10.4208/cicp.scpde14.39s Published online by Cambridge University Press

is a Lyapunov-functional for the process provided $\mathbf{k}_{\text{grav}} \equiv 0$.

Various stable numerical schemes ([13–15]) have been suggested to solve the system (1.1), the convergence of the scheme [13] has been studied in [12]. However, there has been a certain discrepancy between the formulation of the scheme in [13] and its practical realization. Originally formulated in a finite-element setting, the scheme was implemented using a splitting method combining finite-volume-approximations of convective subequations with finite-element approximations of dissipative parts. In the present paper, we intend to overcome this discrepancy by focussing on the stable, uncoupled finite-element splitting scheme that has been proposed in [14]. This scheme essentially differs only by the special form of the convection velocity in the discrete version of (1.1b) from the scheme proposed in [13]. Hence, in the first part of this paper, we will modify and improve the techniques of [12] to prove that appropriate subsequences of discrete solutions to the schemes in [14] converge to a generalized solution in the continuous setting.

We emphasize that – in contrast to [12] – we may allow here for functionals with growth exponent $p = 4$ in $d = 3$ space dimensions, too. This includes e.g. the classical Ginzburg-Landau-functional $F(\varphi) = (1-\varphi^2)^2/4$. In addition, we are able to improve the convergence results of [12] by showing strong convergence for $\nabla\mu$ in $L^2(\Omega_T)$. Moreover, we do not need the condition anymore that the discretization is rectangular in the sense that for each simplicial element $E \in \mathcal{T}_h$, a vertex $x_0(E)$ exists such that all the edges of E touching $x_0(E)$ are vertical to each other. For simulation purposes, it is relevant how the derivative $F'(\cdot)$ is discretized. Reduced acceleration of falling droplets due to numerical dissipation and φ-stability (i.e. non-deviation of φ from $[-1,1]$) are criteria in this respect. In this paper, we prove convergence for a rather large class of discretizations of F' – going beyond the convex-concave splitting considered in [12].

In the second part of the paper, we present numerical experiments in two space dimensions and in three space dimensions for axial-symmetric flow problems. Our computations indicate that a naive approach based on zero numerical dissipation in the double-well potential comes along with non-tolerable φ-deviations – inducing in particular locally negative densities of the kinetic energy $\bar{\rho}(\varphi)|\mathbf{v}|^2/2$, when the Atwood number $\mathfrak{At} := (\tilde{\rho}_2 - \tilde{\rho}_1)/(\tilde{\rho}_1 + \tilde{\rho}_2)$ is sufficiently high. On the other hand, straightforward penalty terms may be introduced which confine φ to the regime $[-\mathfrak{At}^{-1}, \mathfrak{At}^{-1}]$ without changing the falling velocity of the droplet. Finally, we remark that a pure convex-concave splitting reduces the acceleration of falling droplets.

Notation. We consider the two-phase problem on a bounded, convex polygonal (or polyhedral, respectively) domain $\Omega \subset \mathbb{R}^d$ in spatial dimensions $d \in \{2,3\}$. By $\langle \cdot, \cdot \rangle$, we denote the Euclidean scalar product on $\mathbb{R}^d$, and $(\cdot,\cdot)$ is used for the scalar product in $L^2(\Omega)$. Sometimes, we write Ω_T for the space-time cylinder $\Omega \times (0,T)$. By $W^{k,p}(\Omega)$, we denote the space of k-times weakly differentiable functions with weak derivatives in $L^p(\Omega)$. The symbol $W_0^{k,p}(\Omega)$ stands for the closure of $C_0^\infty(\Omega)$ in $W^{k,p}(\Omega)$. Corresponding spaces of vector-valued functions are denoted in boldface. Moreover, we use the function spaces $\mathbf{W}^{1,2}_{0,\text{div}}(\Omega) := \{\mathbf{v} \in \mathbf{W}_0^{1,2}(\Omega) | \operatorname{div} \mathbf{v} = 0\}$, $L_0^2(\Omega) := \{v \in L^2(\Omega) | \int_\Omega v = 0\}$, $H^s(\Omega) := W^{s,2}(\Omega)$,

https://doi.org/10.4208/cicp.scpde14.39s Published online by Cambridge University Press

and $H^1_*(\Omega) := H^1(\Omega) \cap L^2_0(\Omega)$.

For a Banach space X and a time interval I, the symbol $L^p(I;X)$ stands for the parabolic space of L^p-integrable functions on I with values in X. For further notation related to the discretization, we refer the reader to Subsection 2.1.

2 The scheme

2.1 Discretization in space and time

We assume $\mathcal{T}_h$ to be a quasiuniform triangulation of Ω with simplicial elements in the sense of [4].

Concerning discretization with respect to time, we assume that

(T) the time interval $I := [0,T)$ is subdivided in intervals $I_k = [t_k, t_{k+1})$ with $t_{k+1} = t_k + \tau_k$ for time increments $\tau_k > 0$ and $k = 0, \cdots, N-1$. For simplicity, we take $\tau_k \equiv \tau$ for $k = 0, \cdots, N-1$.

For the approximation of both the phase-field φ and the chemical potential μ, we introduce the space U_h of continuous, piecewise linear finite element functions on $\mathcal{T}_h$. The expression $\mathcal{I}_h$ stands for the nodal interpolation operator from $C^0(\Omega)$ to U_h defined by $\mathcal{I}_h u := \sum_{j=1}^{\dim U_h} u(x_j)\theta_j$, where the functions θ_j form a dual basis to the nodes x_j, i.e. $\theta_i(x_j) = \delta_{ij}$, $i,j = 1, \cdots, \dim U_h$.

Let us furthermore introduce the well–known lumped masses scalar product corresponding to the integration formula

$$(\Theta, \Psi)_h := \int_\Omega \mathcal{I}_h(\Theta\Psi).$$

The diagonal, positive definite lumped masses matrix is given by $(M_h)_{ij} = (\varphi_i, \varphi_j)_h$. We recall the following well known estimates:

$$|(u_h, v_h) - (u_h, v_h)_h| \le C h^{1+l} \|u_h\|_l \|v_h\|_1 \qquad \text{for all } u_h, v_h \in U_h, \quad l = 0,1, \tag{2.1}$$

where (u,v) denotes the L^2-scalar product on Ω. In the same spirit, there exist positive constants c, C such that we have for $|\cdot|_h := \sqrt{(\cdot,\cdot)_h}$:

$$c|\cdot|_h^2 \le (\cdot,\cdot) \le C|\cdot|_h^2. \tag{2.2}$$

For the discretization of the velocity field $\mathbf{v}$ and the pressure p, we use function spaces $\mathbf{W}_h \subset \mathbf{X}_h \subset \mathbf{W}^{1,2}_0(\Omega)$ and $S_h \subset L^2_0(\Omega) := \{v \in L^2(\Omega) \,|\, \int_\Omega v = 0\}$ such that the following conditions hold.

(S1) $\mathbf{W}_h := \{\mathbf{v}_h \in \mathbf{X}_h \,|\, \int_\Omega q_h \operatorname{div} \mathbf{v}_h = 0 \quad \forall q_h \in S_h\}$.

https://doi.org/10.4208/cicp.scpde14.39s Published online by Cambridge University Press

(S2) The Babuška-Brezzi condition is satisfied, i.e. a positive constant β exists such that

$$\sup_{\mathbf{v}_h\in\mathbf{X}_h}\frac{(q_h,\mathrm{div}\,\mathbf{v}_h)}{\|\mathbf{v}_h\|_{\mathbf{W}_0^{1,2}(\Omega)}}\geq\beta\|q_h\|_{L^2(\Omega)}$$

for all $q_h\in S_h$.

(S3) The orthogonal L^2-projection $\mathcal{R}_h:\mathbf{L}^2(\Omega)\to\mathbf{W}_h$ is H^1-stable, i.e. a positive constant C exists such that

$$\|\nabla\mathcal{R}_h\mathbf{v}\|_{\mathbf{L}^2(\Omega)}\leq C\|\nabla\mathbf{v}\|_{\mathbf{L}^2(\Omega)} \tag{2.3}$$

for all $\mathbf{v}\in\mathbf{W}_0^{1,2}(\Omega)$. Moreover,

$$\lim_{h\to0}\|\mathcal{R}_h\mathbf{v}-\mathbf{v}\|_{\mathbf{L}^2(\Omega)}=0 \tag{2.4}$$

for all $\mathbf{v}\in\mathbf{W}_{0,\mathrm{div}}^{1,2}(\Omega)$.

(S4) A projection operator $\mathbf{Q}_{\mathrm{div}}^h:\mathbf{W}_{0,\mathrm{div}}^{1,2}(\Omega)\to\mathbf{W}_h$ exists such that

$$\left\|\mathbf{Q}_{\mathrm{div}}^h\mathbf{v}-\mathbf{v}\right\|_{\mathbf{L}^2(\Omega)}+h\left\|\nabla(\mathbf{Q}_{\mathrm{div}}^h\mathbf{v}-\mathbf{v})\right\|_{L^2(\Omega)}\leq Ch^j\|\mathbf{v}\|_{\mathbf{H}^j(\Omega)} \tag{2.5}$$

for all $\mathbf{v}\in\mathbf{H}^j(\Omega)\cap\mathbf{W}_{0,\mathrm{div}}^{1,2}(\Omega)$, $j=1,2$.

(S5) The orthogonal L^2-projection $\mathcal{Q}_h:\mathbf{W}_0^{1,2}(\Omega)\to\mathbf{X}_h$ is H^1-stable.

(S6) The orthogonal L^2-projection $\mathcal{S}_h:L^2(\Omega)\to S_h$ satisfies

$$\lim_{h\to0}\|q-\mathcal{S}_hq\|_{L^2(\Omega)}=0 \tag{2.6}$$

for all $q\in L^2(\Omega)$.

Examples of finite-element spaces $\mathbf{X}_h,S_h$ which comply with (S1) –(S6) are P_2P_1-elements (the so called Taylor-Hood elements) and P_2P_0-elements. In both examples, $\mathbf{X}_h$ is given as

$$\mathbf{X}_h:=\left\{\mathbf{w}\in(\mathbf{C}_0^0(\bar\Omega)):(\mathbf{w})_j|_K\in P_2(K),\,K\in\mathcal{T}_h,\,j=1,\cdots,d\right\},\quad d=2,3.$$

For Taylor-Hood elements, $S_h:=U_h\cap L_0^2(\Omega)$. In the case of P_2P_0-elements,

$$S_h:=\{q_h\in L_0^2(\Omega):q_h|_K\equiv const.\ \ \forall K\in\mathcal{T}_h\}.$$

For more details, we refer the reader to [12].

We conclude this subsection by introducing some more notation. Given a time increment $\tau>0$ (cf. (T)), we will denote the backward (and forward) difference quotients with respect to time by ∂_τ^- (or ∂_τ^+, respectively). Given a subdivision of the time interval

https://doi.org/10.4208/cicp.scpde14.39s Published online by Cambridge University Press

$I:=[0,T)$ with intervals $I_k:=[t_k,t_{k+1})$ as in (T), we introduce $S^{0,-1}([0,T);X)$ associated with a Banach space X as the space of functions $v:[0,T)\to X$ which are constant on each I_k, $k=0,\cdots,N-1$. Given a function $v\in S^{0,-1}([0,T);X)$, we abbreviate $v^k(\cdot):=v(\cdot,t_k)$. In particular, we have

$$\tau\sum_{k=0}^{N-1}v^k(\cdot)=\int_0^T v(\cdot,t)dt. \tag{2.7}$$

In general, we denote functions in $S^{0,-1}(I;U_h)$, $S^{0,-1}(I;\mathbf{W}_h)$, $S^{0,-1}(I;\mathbf{X}_h)$ by an index τh. We often abbreviate $f^k(\cdot):=f_{\tau h}(\cdot,t_k)$.

2.2 The discrete scheme

In this paper, we shall confine ourselves on studying variants of the classical double-well potential

$$F_{class}(\varphi):=\frac{1}{4}(1-\varphi^2)^2=\frac{1}{4}+\frac{1}{4}\varphi^4-\frac{1}{2}\varphi^2.$$

There are various possibilities to discretize $F_{class}(\varphi)$ in such a way that the discrete scheme satisfies an energy estimate similar to (3.1). However, preliminary numerical experiments on falling droplets indicate that there is an intricate interplay between the way, $F_{class}(\cdot)$ is discretized, the time-increment, the positivity of $\bar\rho(\varphi)$, and the falling velocity of the droplet. Heuristically, the falling velocity can be expected to be the larger, the smaller the numerical dissipation is in the scheme.

A straightforward approach to zero numerical dissipation related to the $F_{class}(\cdot)$-contribution to the free energy – suggested in [14] – is to discretize $F'_{class}(\varphi)$ in equation (1.1c) by

$$\begin{aligned}F'_{dis}\left(\varphi^{k+1},\varphi^k\right):=&\frac{F_{class}\left(\varphi^{k+1}\right)-F_{class}\left(\varphi^k\right)}{\varphi^{k+1}-\varphi^k}\\=&\frac{1}{4}\left(\left(\varphi^{k+1}\right)^3+\left(\varphi^{k+1}\right)^2\varphi^k+\varphi^{k+1}\left(\varphi^k\right)^2+\left(\varphi^k\right)^3\right)-\frac{1}{2}\left(\varphi^{k+1}-\varphi^k\right).\end{aligned}$$

This approach has disadvantages. There is no mechanism which enforces φ^{k+1} to stay in (or at least close to) the interval $[-1,1]$. Recall that

$$\bar\rho(\varphi):=\frac{\tilde\rho_2-\tilde\rho_1}{2}\varphi+\frac{\tilde\rho_1+\tilde\rho_2}{2}$$

is positive as long as

$$\varphi>-\frac{\rho_1+\rho_2}{\rho_2-\rho_1}=-\mathfrak{At}^{-1},$$

where the Atwood number $\mathfrak{At}=(\rho_2-\rho_1)/(\rho_1+\rho_2)$ is a measure for the density discrepancy of the fluid components. Note that for air/water - systems $\mathfrak{At}^{-1}\sim 1.002$. Hence, it

https://doi.org/10.4208/cicp.scpde14.39s Published online by Cambridge University Press

seems reasonable to consider

$$F_{pen}(\varphi) := F_{class}(\varphi) + \frac{1}{\delta'} \max\{|\varphi| - 1, 0\}^2$$

instead, where $0 < \delta' \ll 1$ is an appropriately chosen penalty parameter.

Here, we suggest two discretizations, first

$$F'_{dis,pen}(a,b) := F'_{dis}(a,b) + \frac{1}{\delta'} \frac{d}{d\varphi}|_{\varphi=a} \max\{|\varphi| - 1, 0\}^2 \tag{2.8}$$

and secondly

$$F'_{conv,pen}(a,b) := F'_{pen}(a) - \frac{1}{2}(a-b) = F'_+(a) + F'_-\left(\frac{a+b}{2}\right) \tag{2.9}$$

which is intermediate between $F'_{dis,pen}$ and the classical convex-concave splitting $F_{pen}(a,b) = F_+(a) + F_-(b)$ with $F_-(b) = -b^2/2$.

Generically, we will denote the approximation of the derivative of F or of F_{reg} by $F'_{\tau h}$. Note that by standard tools of calculus and convex analysis, the approaches presented above satisfy the following assumptions which will be needed for the analysis of the scheme. Similarly, these assumptions are satisfied by the classical convex-concave splitting of F_{class} or F_{pen}.

Definition 2.1. Let $F \in C^1(\mathbb{R};\mathbb{R}_0^+)$ be given such that F' is piecewise C^1 with at most quadratic growth of the derivatives for $|x| \to \infty$. We call $F'_{\tau h} \in C^0(\mathbb{R}^2;\mathbb{R})$ an admissible discretization of F' if the following is satisfied.

(H1) There is a positive constant C, such that

$$\left|F'_{\tau h}(\varphi,\psi)\right| \le C\left(1 + |\varphi|^3 + |\psi|^3\right).$$

(H2) $F'_{\tau h}(\varphi,\psi)(\varphi - \psi) \ge F(\varphi) - F(\psi)$ for all $\varphi,\psi \in \mathbb{R}$.

(H3) $F'_{\tau h}(\varphi,\varphi) = F'(\varphi)$ for all $\varphi \in \mathbb{R}$.

(H4) There is a positive constant C such that

$$\left|F'_{\tau h}(\varphi,\psi) - F'_{\tau h}(\psi,\theta)\right| \le C\left(\varphi^2 + \psi^2 + \theta^2\right)\left(|\varphi - \psi| + |\psi - \theta|\right)$$

for all $\varphi,\psi,\theta \in \mathbb{R}$.

Let us prove the validity of (H4) for the term F'_{dis}. For the other discretizations listed above, it simply follows by the mean value theorem. We have

$$F'_{dis}(a,b) - F'_{dis}(b,c) = F''_{class}(\lambda\theta_1(a,b) + (1-\lambda)\theta_2(b,c))(\theta_1(a,b) - \theta_2(b,c)),$$

https://doi.org/10.4208/cicp.scpde14.39s Published online by Cambridge University Press

where $\theta_i(\cdot,\cdot)$ are convex combinations of their arguments and λ is contained in $[0,1]$. By convexity of F''_{class} and an appropriate rearrangement of $\theta_1(a,b)-\theta_2(b,c)$, the result follows.

Moreover, we will need the following assumptions on initial data and the regularized mass density $\rho(\varphi)$.

(H5) Let initial data $\Phi_0 \in H^2(\Omega;[-1,1])$ and $\mathbf{V}_0 \in \mathbf{W}^{1,2}_{0,\mathrm{div}}(\Omega)$ be given such that we have for discrete initial data $\varphi_h^0 := \mathcal{I}_h\Phi_0$ and $\mathbf{v}_h^0 := \mathcal{R}_h\mathbf{V}_0$ uniformly in $h>0$ that

$$\int_\Omega \left|\Delta_h\varphi_h^0\right|^2 \leq C\|\Phi_0\|^2_{H^2(\Omega)}$$

and that

$$\int_\Omega \rho(\varphi_h^0)\left|\mathbf{v}_h^0\right|^2 + \frac{1}{2}\int_\Omega \left|\nabla\varphi_h^0\right|^2 + \int_\Omega \mathcal{I}_h F(\varphi_h^0) \leq C\mathcal{E}(\mathbf{V}_0,\Phi_0).$$

Here, the discrete Laplacian $\Delta_h w \in U_h \cap H^1_*(\Omega)$ is defined by

$$(\Delta_h w,\Theta)_h = -\int_\Omega \langle\nabla w,\nabla\Theta\rangle \quad \forall\Theta\in U_h. \tag{2.10}$$

(H6) Given mass densities $0<\tilde\rho_1\leq\tilde\rho_2\in\mathbb{R}$ of the fluids involved and an arbitrary, but fixed regularization parameter $\bar\varphi \in (\frac{\tilde\rho_1}{\tilde\rho_2-\tilde\rho_1}, \frac{2\tilde\rho_1}{\tilde\rho_2-\tilde\rho_1})$, we define the regularized mass density of the two-phase fluid by a smooth, increasing, strictly positive function ρ of the phase-field φ which satisfies

$$\rho(\varphi)|_{(-1-\bar\varphi,1+\bar\varphi)} = \frac{\tilde\rho_2-\tilde\rho_1}{2}\varphi + \frac{\tilde\rho_1+\tilde\rho_2}{2}, \tag{2.11}$$

$$\rho(\varphi)|_{(-\infty,-1-\frac{2\tilde\rho_1}{\tilde\rho_2-\tilde\rho_1})} \equiv const. \tag{2.12}$$

$$\rho(\varphi)|_{(1+\frac{2\tilde\rho_1}{\tilde\rho_2-\tilde\rho_1},\infty)} \equiv const. \tag{2.13}$$

Now, we are in the position to introduce the scheme to be analyzed in this paper. It has been suggested in [14], and it is strongly related to the scheme which has been studied in [13]. The main difference is the choice of convection velocity in the discrete counterpart of (1.1b) which allows to uncouple the momentum equation and the Cahn-Hilliard equation in (1.1). Note that similar splitting ideas have previously been used in [3] and [18] for a model of magnetohydrodynamics and for diffuse interface models for multi-phase flow, respectively. We emphasize that (H1)-(H6), (T), and (S1)-(S6) are assumed to hold. Hence, we discuss rather different discretizations of F' compared to [12]. For the ease of presentation, we assume external forces $\mathbf{k}_{\mathrm{grav}}$ to be zero as these forces are given quantities which enter the system linearly. Hence, they do not have a qualitative effect on estimates and results. Moreover, we assume $M(\varphi)\equiv 1$ and $\sigma=1$, and for initial data, we

https://doi.org/10.4208/cicp.scpde14.39s Published online by Cambridge University Press

skip the index h. We emphasize that it has not been investigated yet whether our technique works for general non-degenerate mobilities $M(\cdot)$. We strongly believe that it does not carry over to degenerate $M(\cdot)$.

Let functions $(\varphi^0,\mathbf{v}^0)\in U_h\times\mathbf{W}_h$ be given. For $k=0,\cdots,N-1$ and given iterates $(\varphi^k,\mu^k,\mathbf{v}^k,p^k)\in U_h\times U_h\times\mathbf{W}_h\times S_h$, we have first to find functions $(\varphi^{k+1},\mu^{k+1})\in U_h\times U_h$ such that

$$\left(\partial_\tau^-\varphi^{k+1},\psi\right)_h-\int_\Omega\varphi^k\left\langle\mathbf{v}^k,\nabla\psi\right\rangle+\tau\int_\Omega\frac{\left|\varphi^k\right|^2}{\rho^k_{\min}}\left\langle\nabla\mu^{k+1},\nabla\psi\right\rangle+\int_\Omega\left\langle\nabla\mu^{k+1},\nabla\psi\right\rangle=0$$
$$\forall\psi\in U_h, \tag{2.14a}$$

$$\left(\mu^{k+1},\psi\right)_h=\int_\Omega\left\langle\nabla\varphi^{k+1},\nabla\psi\right\rangle+\left(\mathcal{I}_h\left(F'_{\tau h}\left(\varphi^{k+1},\varphi^k\right)\right),\psi\right)_h$$
$$+\alpha\int_{\partial\Omega}\partial_\tau^-\varphi^{k+1}\psi+\int_{\partial\Omega}\mathcal{I}_h\left(\frac{\delta\gamma_{LS}}{\delta\varphi}\left(\varphi^{k+1},\varphi^k\right),\psi\right)\qquad\forall\psi\in U_h, \tag{2.14b}$$

and then functions $(\mathbf{v}^{k+1},p^{k+1})\in\mathbf{W}_h\times S_h$ such that

$$\begin{aligned}&\int_\Omega\left\langle\partial_\tau^-(\rho^{k+1}\mathbf{v}^{k+1}),\mathbf{w}\right\rangle-\tfrac{1}{2}\int_\Omega\partial_\tau^-\rho^{k+1}\left\langle\mathbf{v}^{k+1},\mathbf{w}\right\rangle\\&-\tfrac{1}{2}\int_\Omega\rho^k\left\langle\mathbf{v}^k,(\nabla\mathbf{w})^T\mathbf{v}^{k+1}\right\rangle+\tfrac{1}{2}\int_\Omega\rho^k\left\langle\mathbf{v}^k,(\nabla\mathbf{v}^{k+1})^T\mathbf{w}\right\rangle\\&+\tfrac{1}{2}\int_\Omega\rho'(\varphi^{k+1})\left\langle\mathbf{j}^{k+1},(\nabla\mathbf{v}^{k+1})^T\mathbf{w}\right\rangle-\tfrac{1}{2}\int_\Omega\rho'(\varphi^{k+1})\left\langle\mathbf{j}^{k+1},(\nabla\mathbf{w})^T\mathbf{v}^{k+1}\right\rangle\\&+\int_\Omega2\eta(\varphi^{k+1})\mathbf{D}\mathbf{v}^{k+1}:\mathbf{D}\mathbf{w}-\int_\Omega p^{k+1}\operatorname{div}\mathbf{w}\\=&-\int_\Omega\varphi^k\left\langle\nabla\mu^{k+1},\mathbf{w}\right\rangle\qquad\forall\mathbf{w}\in\mathbf{X}_h,\end{aligned} \tag{2.14c}$$

$$\int_\Omega\psi\operatorname{div}\mathbf{v}^{k+1}=0\qquad\forall\psi\in S_h. \tag{2.14d}$$

Note that we define $\rho^k_{\min}:=\min_{\mathbf{x}\in\Omega}\rho\left(\varphi^k(\mathbf{x})\right)$ and that we assume $\delta\gamma_{LS}/\delta\varphi$ to be defined by

$$\frac{\delta\gamma_{LS}}{\delta\varphi}(\varphi,\psi)=\begin{cases}\frac{\gamma_{LS}(\psi)-\gamma_{LS}(\varphi)}{\psi-\varphi}, & \varphi\neq\psi,\\ \gamma'_{LS}(\varphi), & \varphi=\psi.\end{cases}$$

Remark 2.1. In the first line of (2.14a), $\rho^k_{\min}$ may be replaced by ρ^k. As the scheme above is fully uncoupled, existence of discrete solutions easily follows by similar arguments as they are usually applied for Navier-Stokes or Cahn-Hilliard equations separately.

3 Integral estimates

In this section, we show that the discrete counterpart of the physical energy – i.e. the sum of the kinetic and the interfacial energies – acts as a discrete Lyapunov-functional provided no external forces are applied. We start with a local result.

https://doi.org/10.4208/cicp.scpde14.39s Published online by Cambridge University Press

Theorem 3.1. *Assume that the quadruple* $(\varphi^{k+1},\mu^{k+1},\mathbf{v}^{k+1},p^{k+1})$ *solves the system* (2.14) *for given* $(\varphi^k,\mu^k,\mathbf{v}^k)$. *Then,*

$$\begin{aligned}
&\frac{1}{2\tau}\int_\Omega \rho^{k+1}\left|\mathbf{v}^{k+1}\right|^2+\frac{1}{2\tau}\int_\Omega\left|\nabla\varphi^{k+1}\right|^2+\frac{1}{\tau}\int_\Omega \mathcal{I}_h\Big(F\Big(\varphi^{k+1}\Big)\Big)+\frac{1}{\tau}\int_{\partial\Omega}\mathcal{I}_h\Big(\gamma_{LS}\Big(\varphi^{k+1}\Big)\Big)\\
&+\frac{\tau}{4}\int_\Omega \rho^k\left|\partial_\tau^-\mathbf{v}^{k+1}\right|^2+\frac{\tau}{2}\int_\Omega\left|\partial_\tau^-\nabla\varphi^{k+1}\right|^2+\frac{\tau}{3}\int_\Omega\frac{\left|\varphi^k\right|^2}{\rho_{\min}^k}\left|\mathbf{j}^{k+1}\right|^2\\
&+\int_\Omega 2\eta\Big(\varphi^{k+1}\Big)\left|\mathbf{D}\mathbf{v}^{k+1}\right|^2+\int_\Omega\left|\mathbf{j}^{k+1}\right|^2+\alpha\int_{\partial\Omega}\left|\partial_\tau^-\varphi^{k+1}\right|^2\\
\le&\frac{1}{2\tau}\int_\Omega \rho^k\left|\mathbf{v}^k\right|^2+\frac{1}{2\tau}\int_\Omega\left|\nabla\varphi^k\right|^2+\frac{1}{\tau}\int_\Omega \mathcal{I}_h\Big(F\Big(\varphi^k\Big)\Big)+\frac{1}{\tau}\int_{\partial\Omega}\mathcal{I}_h\Big(\gamma_{LS}(\varphi^k)\Big).
\end{aligned}\tag{3.1}$$

Proof. Choosing $\psi:=\partial_\tau^-\varphi^{k+1}$ in (2.14b) and $\psi:=\mu^{k+1}$ in (2.14a) gives together with (H2)

$$\begin{aligned}
&\frac{1}{2\tau}\left[\int_\Omega\left|\nabla\varphi^{k+1}\right|^2-\int_\Omega\left|\nabla\varphi^k\right|^2+\int_\Omega\left|\nabla\varphi^{k+1}-\nabla\varphi^k\right|^2\right]+\frac{1}{\tau}\int_\Omega\mathcal{I}_h\Big(F\Big(\varphi^{k+1}\Big)-F\Big(\varphi^k\Big)\Big)\\
&+\alpha\int_{\partial\Omega}\left|\partial_\tau^-\varphi^{k+1}\right|^2+\frac{1}{\tau}\int_{\partial\Omega}\mathcal{I}_h\Big(\gamma_{LS}\Big(\varphi^{k+1}\Big)-\gamma_{LS}\Big(\varphi^k\Big)\Big)+\int_\Omega\left|\mathbf{j}^{k+1}\right|^2+\tau\int_\Omega\frac{\left|\varphi^k\right|^2}{\rho_{\min}^k}\left|\nabla\mu^{k+1}\right|^2\\
\le&\int_\Omega\varphi^k\Big\langle\mathbf{v}^k,\nabla\mu^{k+1}\Big\rangle.
\end{aligned}\tag{3.2}$$

Testing (2.14c) by $\mathbf{w}=\mathbf{v}^{k+1}$ yields

$$\begin{aligned}
&\frac{1}{2\tau}\left[\int_\Omega\rho^{k+1}\left|\mathbf{v}^{k+1}\right|^2-\int_\Omega\rho^k\left|\mathbf{v}^k\right|^2+\int_\Omega\rho^k\left|\mathbf{v}^{k+1}-\mathbf{v}^k\right|^2\right]+\int_\Omega 2\eta\Big(\varphi^{k+1}\Big)\left|\mathbf{D}\mathbf{v}^{k+1}\right|^2\\
=&-\int_\Omega\varphi^k\Big\langle\mathbf{v}^{k+1},\nabla\mu^{k+1}\Big\rangle.
\end{aligned}$$

Now estimate the terms on the right-hand sides as follows:

$$\int_\Omega\varphi^k\Big(\mathbf{v}^{k+1}-\mathbf{v}^k\Big)\cdot\nabla\mu^{k+1}\ge-\frac{2}{3}\tau\int_\Omega\frac{1}{\rho_{\min}^k}\left|\varphi^k\right|^2\left|\nabla\mu^{k+1}\right|^2-\frac{3}{8\tau}\int_\Omega\rho_{\min}^k\left|\mathbf{v}^{k+1}-\mathbf{v}^k\right|^2$$

Summing up gives the result. □

We immediately obtain the following global result.

https://doi.org/10.4208/cicp.scpde14.39s Published online by Cambridge University Press

Corollary 3.1. *For every $1\le l\le N$ we have*

$$\begin{aligned}
&\frac{1}{2}\int_\Omega \rho^l\left|\mathbf{v}^l\right|^2+\frac{1}{2}\int_\Omega\left|\nabla\varphi^l\right|^2+\int_\Omega \mathcal{I}_h\Big(F\Big(\varphi^l\Big)\Big)+\int_{\partial\Omega}\mathcal{I}_h(\gamma_{LS}(\varphi^l))\\
&+\frac{\tau}{4}\sum_{m=0}^{l-1}\int_\Omega \rho^m\left|\partial_\tau^-\mathbf{v}^{m+1}\right|^2+\frac{\tau}{2}\sum_{m=0}^{l-1}\int_\Omega\left|\partial_\tau^-\nabla\varphi^{m+1}\right|^2+\frac{\tau^2}{3}\sum_{m=0}^{l-1}\int_\Omega\frac{|\varphi^m|^2}{\rho^m_{\min}}|\mathbf{j}^{m+1}|^2\\
&+\tau\sum_{m=0}^{l-1}\int_\Omega 2\eta\Big(\varphi^{m+1}\Big)\left|\mathbf{D}\mathbf{v}^{m+1}\right|^2+\tau\sum_{m=0}^{l-1}\int_\Omega\left|\mathbf{j}^{m+1}\right|^2+\alpha\tau\sum_{m=0}^{l-1}\int_{\partial\Omega}|\partial_\tau^-\varphi^{m+1}|^2\\
\le&\frac{1}{2}\int_\Omega\rho^0\left|\mathbf{v}^0\right|^2+\frac{1}{2}\int_\Omega\left|\nabla\varphi^0\right|^2+\int_\Omega\mathcal{I}_h\big(F(\varphi^0)\big)+\int_{\partial\Omega}\mathcal{I}_h(\gamma_{LS}(\varphi^0)).
\end{aligned}\tag{3.3}$$

Remark 3.1. Note that the term on the right-hand side is just the discrete counterpart of $\mathcal{E}(\mathbf{V}_0,\Phi_0)$ with $\varepsilon=1$.

Let us derive some refined estimates that will entitle us to prove convergence of a subsequence of discrete solutions to a solution in the continuous setting. However, there is so far no proof available for the case $\gamma_{LS}\not\equiv const.$. Therefore, we shall assume $\gamma_{LS}\equiv\alpha=0$ in the sequel.

Lemma 3.1. *Let $(\varphi_{\tau h},\mu_{\tau h},\mathbf{v}_{\tau h},p_{\tau h})$ be a discrete solution of* (2.14) *on $[0,T]$. Then there is a positive constant C_0 depending on $\mathcal{E}(\mathbf{V}_0,\Phi_0)$ and $\int_\Omega\Phi_0$ such that*

$$\|\varphi_{\tau h}\|_{L^4(0,T;L^\infty(\Omega))}\le C_0(1+T).\tag{3.4}$$

Remark 3.2. The proof follows the lines of Lemma 4.1 in [12], but it uses Lemma A.1 instead of Theorem 6.4 in [12]. In particular, it will not be necessary to use triangulations with rectangular simplices as in [12], as our special choice of the double-well potential $F(\cdot)$ permits to bound terms like $(-\Delta_h\varphi^{k+1},F'_{\tau h}(\varphi^{k+1},\varphi^k))_h$ directly.

Proof. Let us prove first that $\Delta_h\varphi_{\tau h}$ is bounded in $L^2(\Omega_T)$. Note the identity

$$-\Big(\Delta_h\varphi^{k+1},\psi\Big)_h=\Big(\mu^{k+1}-F'_{\tau h}(\varphi^{k+1},\varphi^k),\psi\Big)_h\quad\forall\psi\in U_h\tag{3.5}$$

which is a consequence of (2.14b) and the definition (2.10) of the discrete Laplacian. By choosing $\psi=-\Delta_h\varphi^{k+1}$ in (3.5), we have

$$\left\|\Delta_h\varphi^{k+1}\right\|_h\le\left\|\mu^{k+1}-F'_{\tau h}(\varphi^{k+1},\varphi^k)\right\|_h.\tag{3.6}$$

By ((H1)) and (3.3), one has the estimate

$$\left\|F'_{\tau h}(\varphi^{k+1},\varphi^k)\right\|_h^2\le C\Big(1+\|\varphi^{k+1}\|_{L^6}^3+\|\varphi^k\|_{L^6}^3\Big)\le C(1+\mathcal{E}(\mathbf{V}_0,\Phi_0)^{3/2}).\tag{3.7}$$

Then, by applying (3.3), (3.6), (3.7), and integrating with respect to time,

$$\|\Delta_h\varphi_{\tau h}\|^2_{L^2((0,T);L^2(\Omega))}\le\bar{C}(1+T),\tag{3.8}$$

https://doi.org/10.4208/cicp.scpde14.39s Published online by Cambridge University Press

where $\bar{C}>0$ depends on $\mathcal{E}(\mathbf{V}_0,\Phi_0)$. Finally, using the interpolation inequality (A.2), we arrive at

$$\|\varphi_{\tau h}\|^2_{L^4(I;L^\infty(\Omega))}\leq C\mathcal{E}(\mathbf{V}_0,\Phi_0)\tau\sum_{k=0}^{N-1}\left\|\Delta_h\varphi^k\right\|^2_{L^2(\Omega)}+T\mathcal{E}(\mathbf{V}_0,\Phi_0)\leq C(\mathcal{E}(\mathbf{V}_0,\Phi_0))(1+T).$$

The argumentation in dimension $d=2$ is analogous. □

Lemma 3.2. *Let $(\varphi_{\tau h},\mu_{\tau h},\mathbf{v}_{\tau h},p_{\tau h})$ be a discrete solution of (2.14) on $[0,T]$. Then there is a positive constant C_1 depending on $\mathcal{E}(\mathbf{V}_0,\Phi_0)$ such that*

$$\|\Delta_h\varphi_{\tau h}\|_{L^\infty(0,T;L^2(\Omega))}+\|\partial_\tau^-\varphi_{\tau h}\|_{L^2(0,T;L^2(\Omega))}\leq C_1(1+T). \tag{3.9}$$

Remark 3.3. The proof extends the ideas of Theorem 4.2 in [12], considering in particular the additional term

$$\tau\int_\Omega\frac{(\varphi^k)^2}{\rho^k_{\min}}\nabla\mu^{k+1}\cdot\nabla\partial_\tau^-\varphi^{k+1} \tag{3.10}$$

and the class of admissible approximations of $F'(.)$ given in Definition 2.1.

Proof. Using (2.10) to define the discrete Laplacians $\Delta_h\varphi^{k+1}$ and $\Delta_h\varphi^k$ in $U_h\cap H^1_*(\Omega)$, subtracting the corresponding weak formulations from each other and dividing by τ, we have

$$-\left(\partial_\tau^-\Delta_h\varphi^{k+1},\psi\right)_h=\int_\Omega\left\langle\nabla\partial_\tau^-\varphi^{k+1},\nabla\psi\right\rangle\quad\forall\psi\in U_h.$$

Choosing $\psi=\mu^{k+1}$ and using equation (2.14a) entails

$$\begin{aligned}&-\left(\partial_\tau^-\Delta_h\varphi^{k+1},\mu^{k+1}\right)_h+\left(\partial_\tau^-\varphi^{k+1},\partial_\tau^-\varphi^{k+1}\right)_h\\&=\int_\Omega\varphi^k\left\langle\mathbf{v}^k,\partial_\tau^-\nabla\varphi^{k+1}\right\rangle-\tau\int_\Omega\frac{(\varphi^k)^2}{\rho^k_{\min}}\langle\nabla\mu^{k+1},\partial_\tau^-\nabla\varphi^{k+1}\rangle.\end{aligned}$$

The term $\left(\partial_\tau^-\Delta_h\varphi^{k+1},\mu^{k+1}\right)_h$ is rewritten by testing (3.5) by $\psi=\partial_\tau^-\Delta_h\varphi^{k+1}$ as

$$-\left(\partial_\tau^-\Delta_h\varphi^{k+1},\mu^{k+1}\right)_h=\frac{1}{2}\partial_\tau^-(\|\Delta_h\varphi^{k+1}\|_h^2)+\frac{1}{2}\tau\|\partial_\tau^-\Delta_h\varphi^{k+1}\|_h^2-\left(\partial_\tau^-\Delta_h\varphi^{k+1},F'_{\tau h}(\varphi^{k+1},\varphi^k)\right)_h.$$

By adding the two previous equalities, we get

$$\begin{aligned}&\left\|\partial_\tau^-\varphi^{k+1}\right\|_h^2+\frac{1}{2}\partial_\tau^-(\|\Delta_h\varphi^{k+1}\|_h^2)+\frac{1}{2}\tau\|\partial_\tau^-\Delta_h\varphi^{k+1}\|_h^2\\&=-\int_\Omega\left\{\left\langle\mathbf{v}^k,\nabla\varphi^k\right\rangle\partial_\tau^-\varphi^{k+1}+\varphi^k\partial_\tau^-\varphi^{k+1}\operatorname{div}\mathbf{v}^k\right\}+\left(\partial_\tau^-\Delta_h\varphi^{k+1},F'_{\tau h}(\varphi^{k+1},\varphi^k)\right)_h\\&\quad-\tau\int_\Omega\frac{(\varphi^k)^2}{\rho^k_{\min}}\langle\nabla\mu^{k+1},\partial_\tau^-\nabla\varphi^{k+1}\rangle\\&=:R_1^k+R_2^k+R_3^k.\end{aligned} \tag{3.11}$$

https://doi.org/10.4208/cicp.scpde14.39s Published online by Cambridge University Press

Let us take the sum $\tau\sum_{k=0}^{N-1}$ in (3.11) and let us bound the corresponding terms. On the one hand,

$$\left|\tau\sum_{k=0}^{N-1}R_1^k\right|\leq\delta\tau\sum_{k=0}^{N-1}\left\|\partial_\tau^-\varphi^{k+1}\right\|_h^2+C_\delta\tau\sum_{k=0}^{N-1}\left\|\mathbf{v}^k\right\|_{H^1(\Omega)}^2\left(1+\left\|\Delta_h\varphi^k\right\|_h^2\right),\tag{3.12}$$

where we have used the estimate

$$\left\|\nabla\varphi^k\right\|_{L^3(\Omega)}+\left\|\varphi^k\right\|_{L^\infty(\Omega)}\leq C\left(1+\left\|\Delta_h\varphi^k\right\|_h\right)\tag{3.13}$$

which holds according to Theorem 6.4 in [12]. Note that we also took advantage of the fact that $\|\cdot\|_h$ and $\|\cdot\|_{L^2}$ are equivalent norms on U_h with constants uniform in h, see (2.2).

On the other hand, by using the estimate $\left\|\varphi^k\right\|_{L^\infty(\Omega)}\leq C(1+\left\|\Delta_h\varphi^k\right\|_h)$ (see Theorem 6.4 in [12]), one has

$$\begin{aligned}|R_3^k|&\leq C\left\|\varphi^k\right\|_{L^\infty(\Omega)}^2\left\|\nabla\mu^{k+1}\right\|_{L^2(\Omega)}\mathcal{E}(\mathbf{V}_0,\Phi_0)^{1/2}\\&\leq C\left(1+\left\|\Delta_h\varphi^k\right\|_h^2\right)\left\|\nabla\mu^{k+1}\right\|_{L^2(\Omega)}.\end{aligned}$$

Finally, discrete integration by parts with respect to time gives – after a discrete time-integration $\tau\sum_{k=0}^{N-1}$ of (3.11) – for R_2^k

$$\begin{aligned}\tau\sum_{k=0}^{N-1}R_2^k=&-\tau\sum_{k=0}^{N-2}\left(\partial_\tau^+\left(F'_{\tau h}(\varphi^{k+1},\varphi^k)\right),\Delta_h\varphi^{k+1}\right)_h-\left(\Delta_h\varphi^0,F'_{\tau h}(\varphi^1,\varphi^0)\right)_h\\&+\left(\Delta_h\varphi^N,F'_{\tau h}(\varphi^N,\varphi^{N-1})\right)_h\\:=&R_{21}^k+R_{22}^k+R_{23}^k.\end{aligned}\tag{3.14}$$

By using estimate (3.7), we bound the terms R_{22}^k and R_{23}^k as

$$|R_{22}^k+R_{23}^k|\leq C\left(\left\|\Delta_h\varphi^0\right\|_h+\left\|\Delta_h\varphi^N\right\|_h\right)\tag{3.15}$$

with a constant $C=C(\mathcal{E}(\mathbf{V}_0,\Phi_0))$. For R_{21}^k, we use (H4) to obtain

$$\begin{aligned}\left|R_{21}^k\right|\leq&C\tau\sum_{k=0}^{N-2}\left(1+\left\|\varphi^{k+2}\right\|_{L^\infty}^2+\left\|\varphi^{k+1}\right\|_{L^\infty}^2+\left\|\varphi^k\right\|_{L^\infty}^2\right)\\&\cdot\left(\left\|\partial_\tau^-\varphi^{k+2}\right\|_h+\left\|\partial_\tau^-\varphi^{k+1}\right\|_h\right)\left\|\Delta_h\varphi^{k+1}\right\|_h\\\leq&\delta\tau\sum_{k=1}^{N}\left\|\partial_\tau^-\varphi^k\right\|_h^2+C_\delta\tau\sum_{k=0}^{N-2}\left(1+\left\|\varphi^{k+2}\right\|_{L^\infty}^4+\left\|\varphi^{k+1}\right\|_{L^\infty}^4+\left\|\varphi^k\right\|_{L^\infty}^4\right)\left\|\Delta_h\varphi^{k+1}\right\|_h^2.\end{aligned}\tag{3.16}$$

https://doi.org/10.4208/cicp.scpde14.39s Published online by Cambridge University Press

By collecting the bounds (3.12)-(3.16) and taking $\delta>0$ small enough, we get

$$\begin{aligned}
&\frac{1}{4}\left\|\Delta_h\varphi^N\right\|_h^2+\frac{\tau^2}{2}\sum_{k=0}^{N-1}\left\|\partial_\tau^-\Delta_h\varphi^{k+1}\right\|_h^2+\frac{1}{2}\tau\sum_{k=0}^{N-1}\left\|\partial_\tau^-\varphi^{k+1}\right\|_h^2\\
\leq& C(\left\|\Delta_h\varphi^0\right\|_{L^2(\Omega)},\mathcal{E}(\mathbf{V}_0,\Phi_0))+C\tau\sum_{k=0}^{N-1}\left\|\mathbf{v}^k\right\|_{H^1(\Omega)}^2\left(1+\left\|\Delta_h\varphi^k\right\|_h^2\right)\\
&+C(\mathcal{E}(\mathbf{V}_0,\Phi_0))\tau\sum_{k=0}^{N-1}\left\|\nabla\mu^{k+1}\right\|_{L^2(\Omega)}\left(1+\left\|\Delta_h\varphi^k\right\|_h^2\right)\\
&+C\tau\sum_{k=1}^{N-1}\left(1+\left\|\varphi^{k+1}\right\|_{L^\infty(\Omega)}^4+\left\|\varphi^k\right\|_{L^\infty(\Omega)}^4+\left\|\varphi^{k-1}\right\|_{L^\infty(\Omega)}^4\right)\left\|\Delta_h\varphi^k\right\|_h^2. \qquad (3.17)
\end{aligned}$$

By a discrete version of Gronwall's lemma (see e.g. [23, Lemma 4.2.3.]), taking into account the previous estimates and that $\left\|\Delta_h\varphi^0\right\|_h^2\leq C_0$, we infer (3.9). □

4 Passage to the limit $(\tau,h)\to 0$

Now, we are in the position to mimic the argumentation in [12] about the limit behaviour of discrete solutions. We collect the results in the following lemma. Note that we use the notation for discrete functions on space-time cylinders introduced at the end of Section 2.1.

Lemma 4.1. *There is a triple* $(\varphi,\mu,\mathbf{v})$ *with*

$$\begin{aligned}
&\mathbf{v}\in L^\infty\big((0,T);L^2(\Omega)\big)\cap L^2\Big(I;W^{1,2}_{0,\mathrm{div}}(\Omega)\Big),\\
&\varphi\in L^\infty\Big(I;H^1(\Omega)\Big)\cap H^1\big(I;L^2(\Omega)\big),\varphi(\cdot,0)=\Phi_0(\cdot),\\
&\Delta\varphi\in L^\infty((0,T);L^2(\Omega)),\\
&\mu\in L^\infty\big((0,T);L^2(\Omega)\big)\cap L^2\Big(I;W^{1,q}(\Omega)\Big)\cap L^4\Big(I;H^1(\Omega)\Big)
\end{aligned}$$

for every $q<\frac{2d}{d-2}$ *such that for a subsequence* $(\tau,h)\to 0$

$$\begin{aligned}
&(\mathbf{v}_{\tau h})\ \textit{strongly to}\ \mathbf{v}\ \textit{in}\ L^2(\Omega_T)\ \textit{and weakly in}\ L^2\Big(I;\mathbf{W}^{1,2}_0(\Omega)\Big),\\
&(\varphi_{\tau h})\ \textit{strongly to}\ \varphi\ \textit{in}\ L^2(\Omega_T)\ \textit{and weakly in}\ L^\infty\Big(I;H^1(\Omega)\Big)\cap H^1\big(I;L^2(\Omega)\big),\\
&(\Delta_h\varphi_{\tau h})\ \textit{weakly to}\ \Delta\varphi\ \textit{in}\ L^\infty(I;L^2(\Omega)),\\
&(\mu_{\tau h})\ \textit{weakly to}\ \mu\ \textit{in}\ L^2\Big(I;H^1(\Omega)\Big).
\end{aligned}$$

For a proof, we refer to Lemmas 4.3 to 4.8 in [12].

By a passage to the limit in the discrete Cahn-Hilliard equation (2.14a), comparison with its continuous counterpart and lower semi-continuity of the norm under weak convergence, we can show strong convergence of $(\mu_{\tau h})$.

https://doi.org/10.4208/cicp.scpde14.39s Published online by Cambridge University Press

Lemma 4.2. *There is a subsequence* $(\tau,h)\to 0$ *such that* $\nabla\mu_{\tau h}\to\nabla\mu$ *strongly in* $L^2((0,T);\mathbf{L}^2(\Omega))$ *and* $\nabla\varphi_{\tau h}(t)\to\nabla\varphi(t)$ *strongly in* $\mathbf{L}^2(\Omega)$ *for almost every* $t\in(0,T)$.

Proof. Let us first prove that for a subsequence

$$\lim_{(\tau,h)\to 0}\int_\Omega|\nabla\varphi_{\tau h}(t)|^2=\int_\Omega|\nabla\varphi(t)|^2-\int_{\partial\Omega}\varphi(t)\frac{\partial\varphi}{\partial\mathbf{n}} \tag{4.1}$$

for almost all $t\in(0,T)$. Indeed, by Lemma 4.1, there is a subsequence $(\tau,h)\to 0$ such that

- $\varphi_{\tau h}(t)\to\varphi(t)$ strongly in $L^2(\Omega)$ almost everywhere in $(0,T)$,
- $\nabla\varphi_{\tau h}(t)\rightharpoonup\nabla\varphi(t)$ weakly in $\mathbf{L}^2(\Omega)$ almost everywhere in $(0,T)$,
- $\Delta_h\varphi_{\tau h}(t)$ is uniformly bounded in $L^2(\Omega)$ almost everywhere in $(0,T)$.

Hence, using the Ritz projection, (2.1), and (2.10), one easily gets that $\Delta_h\varphi_{\tau h}(t)$ weakly converges to $\Delta\varphi(t)$ in $L^2(\Omega)$ almost everywhere in $(0,T)$. Then (4.1) immediately follows by testing the weak formulation for $\Delta_h\varphi_{\tau h}$ by $\varphi_{\tau h}$ and passing to the limit.

Now, let us consider $\mu_{\tau h}$. Testing the discrete Cahn-Hilliard equation (2.14a) by $\mu_{\tau h}$ and integrating over $(0,t)$, we get

$$\begin{aligned}
&\int_0^t\|\nabla\mu_{\tau h}(.,.+\tau)\|^2_{L^2(\Omega)}\\
=&-\int_0^t\left(\partial_\tau^-\varphi_{\tau h},\mu_{\tau h}(.,.+\tau)\right)_h+\int_{\Omega_t}\varphi_{\tau h}\langle\mathbf{v}_{\tau h}(.,.),\nabla\mu_{\tau h}(.,.+\tau)\rangle\\
&-\tau\int_0^t\int_\Omega\frac{|\varphi_{\tau h}(y,s)|^2}{\rho(\min_{x\in\Omega}\varphi_{\tau h}(x,s))}\langle\nabla\mu_{\tau h}(y,s+\tau),\nabla\mu_{\tau h}(y,s+\tau)\rangle dyds.
\end{aligned}\tag{4.2}$$

Observe that by (2.14b) and (H2)

$$\begin{aligned}
&-\int_0^t\left(\partial_\tau^-\varphi_{\tau h},\mu_{\tau h}(\cdot,\cdot+\tau)\right)_h\\
=&-\int_{\Omega_t}\left\langle\nabla\varphi_{\tau h}(\cdot+\tau),\partial_\tau^-\nabla\varphi_{\tau h}(\cdot+\tau)\right\rangle-\int_0^t\left(\mathcal{I}_h\left(F'_{\tau h}(\varphi_{\tau h}(\cdot+\tau),\varphi_{\tau h}(\cdot))\right),\partial_\tau^-\varphi_{\tau h}(\cdot+\tau)\right)_h\\
\le&-\frac{1}{2}\int_\Omega|\nabla\varphi_{\tau h}(t)|^2+\frac{1}{2}\int_\Omega|\nabla\varphi_{\tau h}(0)|^2-\frac{1}{2}\int_{\Omega_t}|\nabla\varphi_{\tau h}(\cdot+\tau)-\nabla\varphi_{\tau h}(\cdot)|^2\\
&-\int_\Omega\mathcal{I}_hF(\varphi_{\tau h}(t))+\int_\Omega\mathcal{I}_hF(\varphi_{\tau h}(0)).
\end{aligned}$$

For the third term on the right-hand side, we have the bound

$$\begin{aligned}
\int_{\Omega_t}|\nabla\varphi_{\tau h}(\cdot+\tau)-\nabla\varphi_{\tau h}(\cdot)|^2&=-\tau\int_0^t\left(\Delta_h(\varphi_{\tau h}(\cdot+\tau)-\varphi_{\tau h}(\cdot)),\varphi_{\tau h}(\cdot+\tau)-\varphi_{\tau h}(\cdot)\right)_h\\
&\le 2\tau\|\Delta_h\varphi_{\tau h}\|_{L^2((0,t);L^2(\Omega))}\left\|\partial_\tau^-\varphi_{\tau h}(\cdot+\tau)\right\|_{L^2(\Omega_t)}\\
&=\mathcal{O}(\tau)
\end{aligned}$$

https://doi.org/10.4208/cicp.scpde14.39s Published online by Cambridge University Press

by (2.10) and Lemma 3.2.

For the fourth term on the right-hand side, we have

$$\lim_{(\tau,h)\to 0}\int_\Omega \mathcal{I}_h F(\varphi_{\tau h}(t)) = \int_\Omega F(\varphi(t))$$

for almost every $t\in(0,T)$ due to the strong convergence of $\varphi_{\tau h}$ in $L^4(\Omega_T)$ and the fact that $L^p(I;L^p(\Omega))$-convergence entails convergence in $L^p(\Omega)$ for almost every t for an appropriate subsequence.

The convergence of the second term on the right-hand side of (4.2) follows using the strong convergence of $\mathbf{v}_{\tau h}$ and $\varphi_{\tau h}$ combined with the weak convergence of $\nabla\mu_{\tau h}$, see Lemma 4.1. The vanishing of the last term on the right-hand side is a direct consequence of the uniform boundedness of $\varphi_{\tau h}$ and $\nabla\mu_{\tau h}$ in $L^\infty(\Omega_T)$ and $L^2(\Omega_T)$, respectively. Hence, taking the limit inferior on both sides of (4.2) and using the lower semi-continuity of the norm with respect to weak convergence, we get for an appropriate subsequence $(\tau,h)\to 0$ which will not be relabeled

$$\begin{aligned}
&\frac{1}{2}\int_\Omega |\nabla\varphi(t)|^2 + \int_0^t \|\nabla\mu(\cdot)\|^2_{L^2(\Omega)}\\
\le&\liminf_{(\tau,h)\to 0}\left(\frac{1}{2}\int_\Omega |\nabla\varphi_{\tau h}(t)|^2 + \int_0^T \|\nabla\mu_{\tau h}(\cdot+\tau)\|^2_{L^2(\Omega)}\right)\\
\le&\frac{1}{2}\int_\Omega |\nabla\Phi_0|^2 - \int_\Omega F(\varphi(t)) + \int_\Omega F(\Phi_0) + \iint_{\Omega_T}\varphi\langle\mathbf{v},\nabla\mu\rangle
\end{aligned}$$

for almost every $t\in(0,T)$. Now passing to the limit $(\tau,h)\to 0$ in the equation (2.14a), using again Lemma 4.1, and testing by μ gives the identity

$$\frac{1}{2}\int_\Omega |\nabla\varphi(t)|^2 - \frac{1}{2}\int_\Omega |\nabla\Phi_0|^2 + \int_\Omega F(\varphi(t)) - \int_\Omega F(\Phi_0) + \int_{\Omega_t}\varphi\langle\mathbf{v},\nabla\mu\rangle + \int_{\Omega_t}|\nabla\mu|^2 = 0.$$

Hence,

$$\liminf_{(\tau,h)\to 0}\left(\frac{1}{2}\|\nabla\varphi_{\tau h}(t)\|^2_{L^2(\Omega)} + \|\nabla\mu_{\tau h}\|^2_{L^2(\Omega_t)}\right) = \frac{1}{2}\|\nabla\varphi(t)\|^2_{L^2(\Omega)} + \|\nabla\mu\|^2_{L^2(\Omega_t)^2} \tag{4.3}$$

for almost every $t\in(0,T)$. Let us now prove that $\int_{\partial\Omega}\varphi\frac{\partial\varphi(t)}{\partial\mathbf{n}} = 0$. By (4.1), the weak convergence of $\nabla\varphi_{\tau h}(t)$ and the lower semi-continuity of the norm, we find

$$\int_{\partial\Omega}\varphi(t)\frac{\partial\varphi}{\partial\mathbf{n}} \le 0 \tag{4.4}$$

almost everywhere in $(0,T)$. Combining (4.3) with (4.1) and using the weak convergence of $\nabla\mu_{\tau h}$ entails

$$\int_{\partial\Omega}\varphi\frac{\partial\varphi(t)}{\partial\mathbf{n}} = \liminf_{(\tau,h)\to 0}\int_0^t \|\nabla\mu_{\tau h}(\cdot+\tau)\|^2_{L^2(\Omega)} - \int_0^t \|\nabla\mu(\cdot)\|^2_{L^2(\Omega)} \ge 0.$$

https://doi.org/10.4208/cicp.scpde14.39s Published online by Cambridge University Press

Hence, $\int_\Omega |\nabla\varphi_{\tau h}(t)|^2 \to \int_\Omega |\nabla\varphi(t)|^2$ almost everywhere in $(0,T)$, which implies the strong convergence of $\nabla\varphi_{\tau h}$. By (4.3), we infer $\lim_{(\tau,h)\to 0}\|\nabla\mu_{\tau h}\|_{L^2(\Omega_t)} = \|\nabla\mu\|_{L^2(\Omega_t)}$, first almost everywhere in $(0,T)$, then by density on the whole interval. □

This result may also be used for the passage to the limit $(\tau,h)\to 0$ in the fifth term on the left-hand side of (2.14c).

Taking into account that – different from the approach in [12] – the terms involving $\mathbf{j}^{k+1}$ in (2.14c) have the prefactor $\rho'(\varphi^{k+1})$ instead of $(\tilde\rho_2-\tilde\rho_1)/2$, we may combine Theorem 5.2 and Corollary 5.4 in [12] to end up with the following result.

Theorem 4.1. *Let $\Omega\subset\mathbb{R}^d$, $d\in\{2,3\}$ be a convex polyhedral domain and let initial data Φ_0 and $\mathbf{V}_0$ be given. Let $I=(0,T)$. Assume that hypotheses* (H1)-(H6), (T) *and* (S1)-(S6) *are satisfied and that $(\varphi_{\tau h},\mu_{\tau h},\mathbf{v}_{\tau h})$ is a sequence of discrete solutions to the system* (2.14). *Then the functions $(\mathbf{v},\varphi,\mu)$ constructed in Lemma* 4.1 *solve the system* (1.1) *in the sense that*

$$\begin{aligned}
&-\iint_{\Omega_T}\langle\rho\mathbf{v}-\rho(\Phi_0)\mathbf{V}_0,\partial_t\mathbf{w}\rangle-\iint_{\Omega_T}\partial_t\rho\langle\mathbf{v},\mathbf{w}\rangle+\iint_{\Omega_T}\rho\Big\langle\mathbf{v},(\nabla\mathbf{v})^T\mathbf{w}\Big\rangle\\
&+\iint_{\Omega_T}\frac{\partial\rho}{\partial\varphi}\Big\langle\mathbf{j},(\nabla\mathbf{v})^T\mathbf{w}\Big\rangle+\iint_{\Omega_T}2\eta(\varphi)\mathbf{D}\mathbf{v}:\mathbf{D}\mathbf{w}\\
=&\iint_{\Omega_T}\mu\langle\nabla\varphi,\mathbf{w}\rangle
\end{aligned}\tag{4.5}$$

for all $\mathbf{w}\in C(I;W^{1,2}_{0,\mathrm{div}}(\Omega))$ satisfying $\mathbf{w}(\cdot,T)=0$.

Remark 4.1. Note that the regularisation ρ can be replaced by $\bar\rho(\varphi)=\frac{1}{2}(\tilde\rho_2+\tilde\rho_1)+\frac{1}{2}(\tilde\rho_2-\tilde\rho_1)\varphi$, as long as φ remains in the linear regime of $\rho(\cdot)$ which is given by $[-\mathfrak{At}^{-1}+\epsilon,\mathfrak{At}^{-1}-\epsilon]$ where $\mathfrak{At}:=(\tilde\rho_2-\tilde\rho_1)/(\tilde\rho_1+\tilde\rho_2)$ is the Atwood number. Due to (3.9), this is always true locally in time for physically admissible initial data.

5 Numerical experiments

In first, unpublished simulations using the presented spitting schemes together with the classical convex-concave splitting of F_{pen}, we discovered a significant deviation of the falling velocity compared to simulations based on the scheme proposed in [13]. In particular, the droplet simulated on the basis of the splitting scheme fell more slowly, when using large time increments. This deviation vanished for small time increments. Therefore, we developed approximations for F' with reduced numerical dissipation. In the following subsections, we will examine these schemes with respect to their dependence on the time increment τ, the effect of the different amount of numerical dissipation on the falling velocity and boundedness of the phase field. Although the underlying model is based on the assumption that φ is confined to the interval $[-1,1]$, there is no mechanism which ensures this assumption when a polynomial double-well potential is used and the mobility is non-degenerate. As a result the regularisation of $\bar\rho$ is necessary.

https://doi.org/10.4208/cicp.scpde14.39s Published online by Cambridge University Press

For the readers convenience, we recall the presented schemes:

Scheme 1

$$F_{class}(\varphi)=\frac{1}{4}\left(1-\varphi^2\right)^2,$$
$$F'_{dis}(\varphi,\psi)=\frac{F_{class}(\varphi)-F_{class}(\psi)}{\varphi-\psi}=\frac{1}{4}\left(\varphi^3+\varphi^2\psi+\varphi\psi^2+\psi^3\right)-\frac{1}{2}(\varphi+\psi).$$

Scheme 2

$$F_{pen}(\varphi)=\frac{1}{4}\left(1-\varphi^2\right)^2+\frac{1}{\delta'}\max\{|\varphi|-1,0\}^2,$$
$$F'_{dis,pen}(\varphi,\psi)=F'_{dis}(\varphi,\psi)+\frac{1}{\delta'}\frac{d}{d\theta}|_{\theta=\varphi}\max\{|\theta|-1,0\}^2.$$

Scheme 3

$$F_{pen}(\varphi)=\tfrac{1}{4}\left(1-\varphi^2\right)^2+\frac{1}{\delta'}\max\{|\varphi|-1,0\}^2,$$
$$F'_{conv,pen}(\varphi,\psi)=F'(\varphi)-\frac{1}{2}F''_{-}(\psi)(\varphi-\psi).$$

The amount of numerical dissipation may be influenced by the choice between $\rho\left(\varphi^k\right)$ or $\rho^k_{\min}$ in (2.14a). In the following we will denote Scheme X with $\rho^k_{\min}$ in (2.14a) by Scheme Xa and the according version with ρ^k by Scheme Xb. While the a-versions of the schemes can be implemented easily without causing any errors due to quadrature rules, they are still a coarser approximation than the versions using ρ^k. Therefore one may hope that the b-schemes yield better results.

For practical computations, we use the inhouse code EconDrop developed by G. Grün, F. Klingbeil and S. Metzger with contributions of H. Grillmeier (see [13], and also [2, 5, 9]). This framework allows for adaptivity in space and time. We refer to [13] for details. For further reference, we recall that the time increment τ is controlled by the ratio

$$\frac{\text{grid size}}{\text{propagation speed of the interface}}.$$

The propagation speed of the interface v^k_{int} is approximated by

$$v^k_{\text{int}}:=\max\left|\mathbf{v}^k\right|+\max\left|M\left(\varphi^k\right)\frac{\nabla\mu^k}{\max\{|\varphi^k|,0.1\}}\right|. \tag{5.1}$$

This yields a time increment

$$\tau_{k+1}=C_\tau\frac{h_{\min}}{v^k_{\text{int}}}, \tag{5.2}$$

https://doi.org/10.4208/cicp.scpde14.39s Published online by Cambridge University Press

with a positive constant $C_\tau < 1$.

In previous publications on the comparison of different phase-field models or different discretization methods, often test cases have been considered for which the schemes behaved equally well. Here, we focus on a setting which has been suggested already in [13] and which may be used to disclose differences. We choose Atwood numbers of 0.99 or 0.999 which correspond to mass density ratios of 199 or 1999. Then we monitor the falling of a droplet of high mass density assuming that both liquids have the same viscosity – see Fig. 1. Our computational domain is $[0,1]\times[0,2]$, the barycenter of the droplet is initially located at $(0.5,1.5)$, the droplet's diameter is 1. The non-dimensionalized acceleration is given by 10^4, the corresponding force is directed in negative y-direction.

What is special about this setting? The model (1.1) differs only by the **j**-term in the momentum equation from the model suggested in [7]. Observe that **j** is (in the case of constant mobilities) proportional to the gradient of the chemical potential μ which itself is the first variation of the interfacial energy $A_\varepsilon(\varphi) := \int_\Omega \frac{\varepsilon}{2}|\nabla\varphi|^2 + \int_\Omega \frac{1}{\varepsilon}F(\varphi)$. As explained in [19,20], see also [13], $A_\varepsilon(\varphi)$ is a diffuse interface approximation of the $(d-1)$-dimensional Hausdorff measure of the level set $[\varphi=0]$ which plays the role of the liquid-liquid interface. Recalling that the first variation of area is given by mean curvature and that the chemical potential μ is the first variation of $A_\varepsilon(\cdot)$, **j** can heuristically be related to curvature gradients. Therefore, one should look for a setting with self-propelling tip formations when searching for experimental settings where the proven stability of (1.1) may yield advantages compared to the model in [7]. In fact, unpublished numerical experiments based on the model proposed in [7] turn out to become unstable in this setting. Therefore, we expect this setting to be a good choice to compare different versions of our scheme.

At the liquid-solid interface, we have the choice between no-slip or Navier-slip boundary conditions. Since the domain Ω is rather small, we prefer Navier-slip to minimize boundary effects (i.e., we only prescribe $\mathbf{v}\cdot\mathbf{n}=0$ on $\partial\Omega$ instead of $\mathbf{v}=0$). The velocity field is discretized by Taylor–Hood elements. Concerning the remaining parameters, we pick $\delta' = 4\cdot 10^{-3}$, $\varepsilon = 0.025$, $\sigma = 2$, $M = 0.005$ and $h = 0.0156$ in the interface region and $h = 0.0221$ in the bulk.

5.1 Experimental order of convergence

In the first subsection, we investigate the dependence of Scheme 3 on the time increment. In particular, we will compare the experimental order of convergence with respect to the time increment for Scheme 3a and Scheme 3b. We observe that Scheme 3b yields better results, but it is still sensitive with respect to the time increment. In a first series of experiments, we choose $\mathfrak{At}=0.99$ and compare Scheme 3a and Scheme 3b for varying C_τ. Fig. 1 shows the evolution of the droplet. Note the characteristic liquid jet, which turns up at the beginning of the experiment.

It would be intriguing to find out whether we are observing the formation of a tip or even of a cusp. A definite answer seems to be beyond the resolution depth of phase-field

https://doi.org/10.4208/cicp.scpde14.39s Published online by Cambridge University Press



Figure 1: Position and shape of the droplet ($\mathfrak{At}=0.99$) at time $t=0$, $t=0.007$, $t=0.0085$, $t=0.011$, $t=0.017$, $t=0.02$ (computed using Scheme 3b, $C_\tau=0.1$).

Table 1: φ-deviation at $t=0.007$ in $\|\cdot\|_{L^2(\Omega)}$ and in $\|\cdot\|_{L^\infty(\Omega)}$ for various values of C_τ against the reference solution with $C_\tau=0.01$ ($\mathfrak{At}=0.99$). Last line: φ-deviation of the mixed FE-FV-scheme of [13] for C_τ.

	Scheme 3a		Scheme 3b	
C_τ	L^2	L^∞	L^2	L^∞
0.90	$2.907\cdot10^{-1}$	$1.461\cdot10^{0}$	$1.772\cdot10^{-1}$	$1.029\cdot10^{0}$
0.50	$1.802\cdot10^{-1}$	$1.022\cdot10^{0}$	$1.062\cdot10^{-1}$	$6.675\cdot10^{-1}$
0.10	$5.632\cdot10^{-2}$	$3.795\cdot10^{-1}$	$2.483\cdot10^{-2}$	$1.761\cdot10^{-1}$
0.05	$3.122\cdot10^{-2}$	$2.160\cdot10^{-1}$	$1.317\cdot10^{-2}$	$9.527\cdot10^{-2}$
0.9 (scheme of [13])	$3.127\cdot10^{-2}$	$2.660\cdot10^{-1}$	$2.772\cdot10^{-2}$	$2.276\cdot10^{-1}$

Table 2: φ-deviation at $t=0.0085$ in $\|\cdot\|_{L^2(\Omega)}$ and in $\|\cdot\|_{L^\infty(\Omega)}$ for various values of C_τ against the reference solution with $C_\tau=0.01$ ($\mathfrak{At}=0.99$). Last line: φ-deviation of the mixed FE-FV-scheme of [13] for C_τ.

	Scheme 3a		Scheme 3b	
C_τ	L^2	L^∞	L^2	L^∞
0.90	$2.664\cdot10^{-1}$	$1.158\cdot10^{0}$	$1.820\cdot10^{-1}$	$1.018\cdot10^{0}$
0.50	$1.679\cdot10^{-1}$	$8.013\cdot10^{-1}$	$1.080\cdot10^{-1}$	$6.463\cdot10^{-1}$
0.10	$5.732\cdot10^{-2}$	$3.895\cdot10^{-1}$	$2.360\cdot10^{-2}$	$1.579\cdot10^{-1}$
0.05	$3.306\cdot10^{-2}$	$2.414\cdot10^{-1}$	$1.215\cdot10^{-2}$	$8.279\cdot10^{-2}$
0.9 (scheme of [13])	$3.320\cdot10^{-2}$	$2.234\cdot10^{-1}$	$3.355\cdot10^{-2}$	$1.795\cdot10^{-2}$

methods. The fact that the analysis of the corresponding free surface problem is just in its very childhood prevents us from contributing to this discussion.

Using the computations based on $C_\tau=0.01$ as a reference solution, we study the errors of the phase-field measured in the L^2- and L^∞-norm. The absolute errors at $t=0.007$ and $t=0.0085$ can be found in Table 1 and Table 2. Altogether, we achieve experimental orders of convergence of 0.91 (L^2) and 0.84 (L^∞) for Scheme 3b and 0.77 (L^2) and 0.63 (L^∞) for the numerically cheaper Scheme 3a, which indicates the better performance of Scheme 3b.

https://doi.org/10.4208/cicp.scpde14.39s Published online by Cambridge University Press

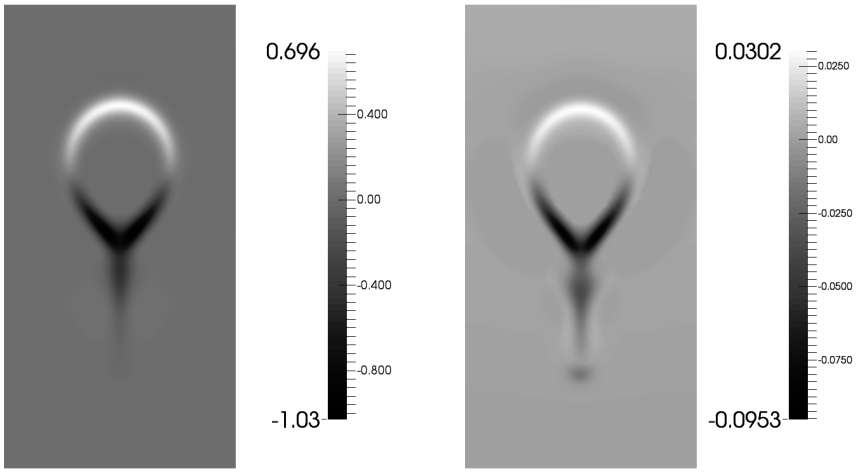


Figure 2: Scheme 3b, $\mathfrak{At}=0.99$: φ-deviation at time $t=0.007$ for values of $C_\tau=0.9$ (left) and $C_\tau=0.05$ (right).

It is worth mentioning that the L^∞-error mirrors different falling velocities of the droplets. Fig. 2 shows the φ-deviation from the reference solution. The dark area around the tip of the droplet indicates that the reference droplet falls faster. The magnitude of the difference indicates that the deviation of the droplet positions between the simulations using $C_\tau=0.9$ and $C_\tau=0.01$ is about half of the width of the interface (see left part of Fig. 2). The right part of Fig. 2 indicates that decreasing C_τ reduces the deviation.

The results give evidence that the phase field computed using Scheme 3a and Scheme 3b converges for $C_\tau \searrow 0$. Nevertheless, time increments with $\mathcal{C}_\tau$ close to one may give false results on droplet motion.

It is interesting to compare the results presented here with the scheme in [13] which is a mixed FE-FV-scheme. In particular, it uses a second order finite volume scheme for the convective parts. Note that good results are already obtained for $C_\tau=0.9$ (see Tables 1, 2). Observe, however, that large time increments do not come for free. The scheme in [13] uses in each time-step inner iterations which are time-consuming. Moreover, instabilities at the tip of the jet may arise when using large time increments (see Fig. 3).

5.2 Impact of discretizations on φ-stability and droplet motion

This subsection is devoted to the comparison of the schemes Scheme 1-Scheme 3 regarding φ-stability and droplet motion – or more precisely, the falling velocity of the droplets. We present simulations showing that some kind of penalty term is necessary to confine φ to an acceptable range, i.e. a closed subinterval of $(-\mathfrak{At}^{-1},\mathfrak{At}^{-1})$, which is essentially the regime where $\rho(\varphi)$ stays linear. We want to emphasize that in our setting, we have to confine φ to a closed subinterval of $(-1.\overline{01},1.\overline{01})$ for $\mathfrak{At}=0.99$ and $(-1.\overline{001},1.\overline{001})$ for $\mathfrak{At}=0.999$, respectively. If it is not possible to confine φ to this interval, we need the afore-

https://doi.org/10.4208/cicp.scpde14.39s Published online by Cambridge University Press

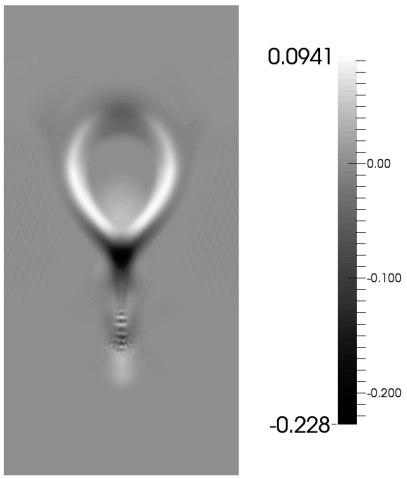


Figure 3: $\mathfrak{At}=0.99$: φ-deviation at time $t=0.007$ between Scheme 3b with $C_\tau=0.01$ and the scheme proposed in [13] with $C_\tau=0.9$.

mentioned regularisation ρ. Otherwise we lose the positivity of $\bar{\rho}$ and the well-posedness of our problem. Secondly we give strong indication that reduced numerical dissipation leads to higher falling velocities. In this subsection, we confine ourselves to the b-versions of the schemes 1-3. We fix $C_\tau=0.1$ and use $\mathfrak{At}=0.99$ and $\mathfrak{At}=0.999$.

The minimum and maximum values of φ for $\mathfrak{At}=0.99$ are plotted in Fig. 4. It turns out that for our set of parameters the penalty function with $\delta'=4\cdot10^{-3}$ is sufficient to control the modulus of φ and to use a linear mass density function. Comparing the evolution of the droplet (see Fig. 1 and Fig. 4), we note that in the computations based on Scheme 1 the maximum of φ grows until the jet touches the bottom of the domain. The minimum of φ shrinks until the droplet also reaches the bottom. In particular, φ attains negative values outside the interval $[-1.\overline{01},1.\overline{01}]$ already for values of $t<0.0065$. For late times of the simulation, coincidentally with the impact at the bottom of the computational domain, the droplet starts to dissolve. As a result, the maximum values of φ fall below 1 for all schemes. Similar results can be observed for $\mathfrak{At}=0.999$ (see Fig. 5). The slight deviation of $\min\varphi$ at the beginning of the simulation arises as our initial data do not represent the exact energetic minimum of the phase field. This effect was also observed and explained in [24].

Again, comparing the simulations based on Scheme 2b and Scheme 3b indicates a slight deviation in the position of the droplets. More precisely, the droplet based on the less dissipative scheme falls faster (cf. Fig. 6).

5.3 Droplets on inclined planes with general contact angles

In this subsection, we present simulations for scheme (2.14) with $\gamma_{LS}\neq0$. We are interested in qualitative results for preceding and receding macroscopic contact angles in

https://doi.org/10.4208/cicp.scpde14.39s Published online by Cambridge University Press

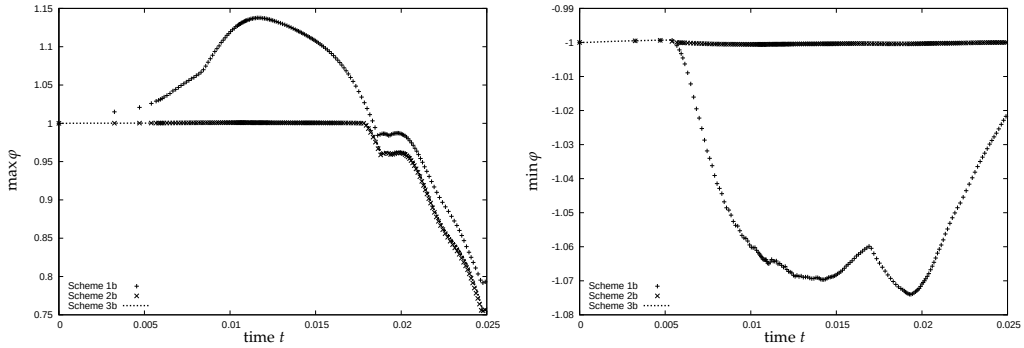


Figure 4: Comparison of the extrema of φ for $\mathfrak{At}=0.99$ for the different schemes.

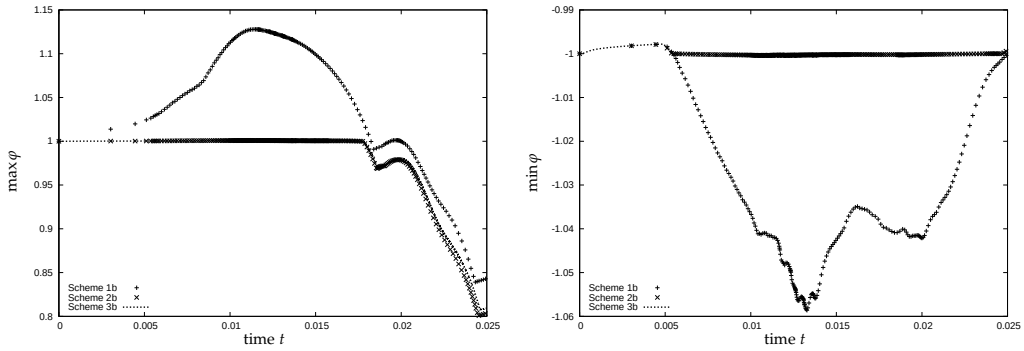


Figure 5: Comparison of the extrema of φ for $\mathfrak{At}=0.999$ for the different schemes.

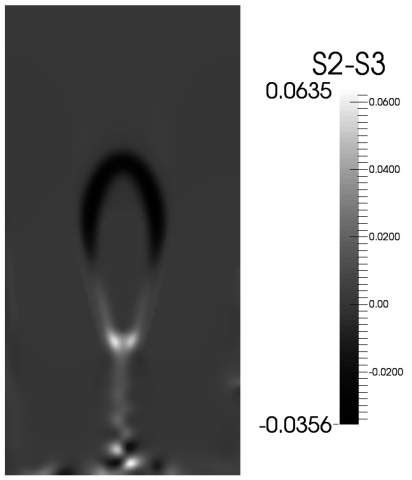


Figure 6: φ-deviation between Scheme 2b and Scheme 3b at time $t=0.0112$.

https://doi.org/10.4208/cicp.scpde14.39s Published online by Cambridge University Press

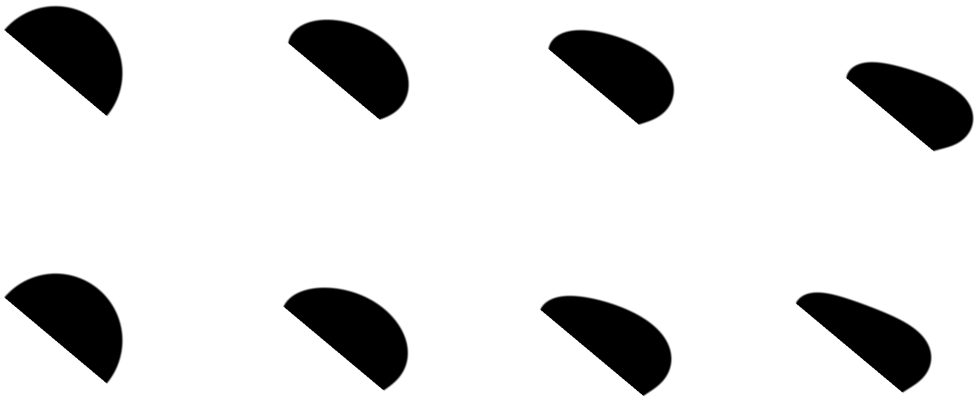


Figure 7: Droplets on an inclined plane at $t=0$, $t=0.4$, $t=1$, $t=8$ with $\Delta\gamma_{LS}=0.4$ (above) and $\Delta\gamma_{LS}=0.2$ (below).

droplet flow downwards an inclined plane. We study a droplet sliding down an infinite inclined plane with an inclination angle of 40°. For this, we consider a computational domain $[0,6]\times[0,2]$ and we apply a non-dimensionalized gravitational acceleration of $(10\sin(\frac{2}{9}\pi),-10\cos(\frac{2}{9}\pi))^T$. At the boundary portions given by $x=0$ and by $x=6$, we take periodic boundary conditions while at the portions $y=0$ and $y=2$ the conditions of (1.2a) hold true. For this series of experiments, we have chosen $\delta'=10^{-3}$, $\varepsilon=0.01$, $M=0.01$ and $\sigma=0.8$. The droplet under consideration has the mass density 1 and the viscosity 0.05 while the ambient liquid is of mass density 0.1 and viscosity of 0.5. Initially the droplet has a hemicircular shape with contact angle of 90° and a diameter of 1. It is placed at $(0.7,0.0)$. To define the contact angle, we use a deviation in the liquid-solid interfacial energy densities γ_{LS} of $\Delta\gamma_{LS}=0.4$ or $\Delta\gamma_{LS}=0.2$ (cf. (1.4)). Using the relation

$$\cos(\theta)=-\frac{\Delta\gamma_{LS}}{\sigma}, \tag{5.3}$$

we obtain a contact angle θ of 120° (or about 104° for $\Delta\gamma_{LS}=0.2$). For our simulations we used an adaptive grid ($h=0.0442$ in the bulk region and $h=0.0039$ in the interface) and a fixed time increment of $\tau=0.001$. In these simulations velocity and pressure are discretized using stabilized P1P1 elements (see e.g. [8]). As shown in Fig. 7, the droplet rapidly attains the microscopically prescribed contact angle. Macroscopically, the receding angle is smaller than the equilibrium angle. Microscopic contact angle hysteresis cannot be expected as α has been chosen to be zero.

5.4 3D falling droplets: Case of rotational symmetry

In this subsection we present a 3D axial symmetric simulation of an initially ball-shaped falling droplet. The droplet phase is characterized by values 20 and 0.5 of mass density and viscosity, respectively, while 0.1 and 0.05 are the corresponding values of the

https://doi.org/10.4208/cicp.scpde14.39s Published online by Cambridge University Press

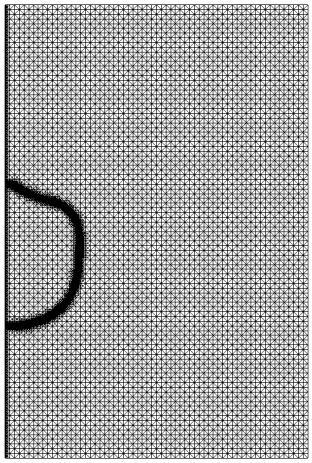


Figure 8: Mesh used for the computations of Fig. 9 ($t=0.4$).

ambient liquid. For $(M,\sigma,\varepsilon,\delta')$, we take $(0.01,0.3,0.007,0.004)$. The non-dimensionalized gravitational acceleration is given by 10. It is pointing in negative y-direction. Exploiting the rotational symmetry, we used cylindrical coordinates and the computational domain $[0,2]\times[0,3]$. The simulation is initiated with a circular droplet of diameter 1 placed with its barycenter at $(0,2)$. In this simulation, velocity and pressure are discretized using stabilized P1P1 elements (see e.g. [8]). For our simulation we used an adaptive grid ($h=0.0442$ in the bulk region and $h=0.0039$ in the interface) and a fixed time increment of $\tau=0.0001$. Regarding the adaptivity in space, we use the ideas presented in [13], resulting in a mesh as displayed in Fig. 8. Note the high resolution in the interfacial area.

The result of the simulation can be seen in Fig. 9. At the impact the droplet changes its topological shape forming an anulus.

A Appendix

A.1 Discrete Gagliardo-Nirenberg-Inequality

Lemma A.1. *Let $\mathcal{T}_h$ be a quasi-uniform triangulation of the polyhedral domain $\Omega\subset\mathbb{R}^3$ in the sense of* [4]. *We assume $A_h: U_h\to U_h\cap H^1_*(\Omega)$ to be defined by*

$$(A_h\phi,\psi)=\int_\Omega \nabla\phi\cdot\nabla\psi \qquad \text{for all } \psi\in U_h. \tag{A.1}$$

Then there is a positive constant C, such that

$$\|\chi\|_{L^\infty(\Omega)}\leq C\|A_h\chi\|^{\frac{1}{2}}_{L^2(\Omega)}\|\chi\|^{\frac{1}{2}}_{H^1(\Omega)}+\|\chi\|_{H^1(\Omega)} \qquad \text{for all } \chi\in U_h. \tag{A.2}$$

https://doi.org/10.4208/cicp.scpde14.39s Published online by Cambridge University Press

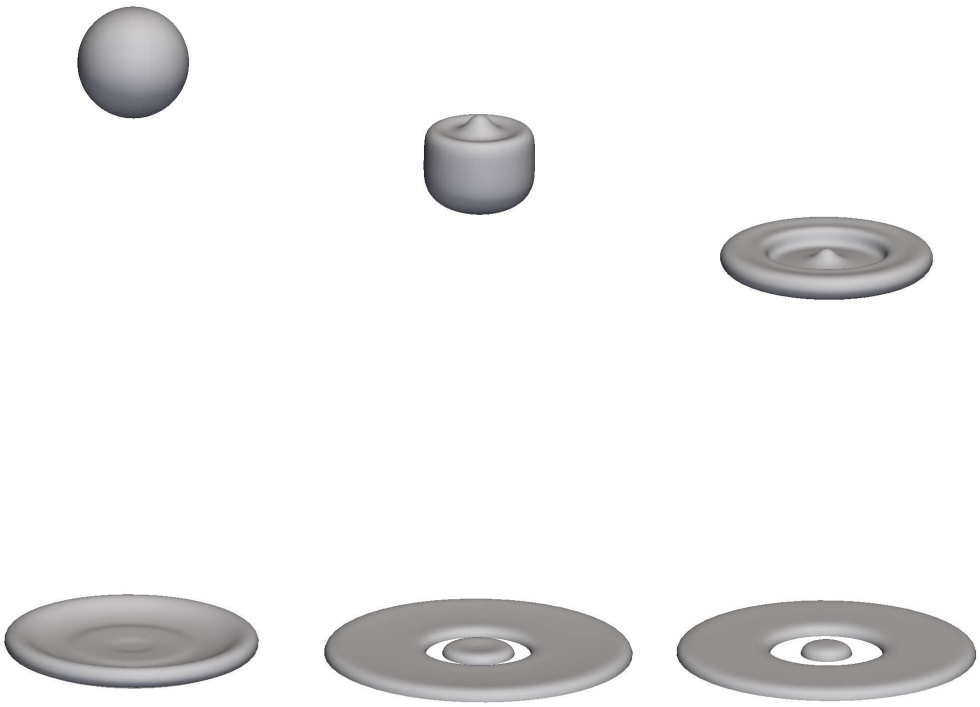


Figure 9: Falling droplet at $t=0$, $t=0.5$, $t=0.95$, $t=1.1$, $t=1.5$ and $t=2.5$.

Proof. The argument is inspired by the methods of [16]. Let us show that for $\phi \in U_h \cap H^1_*(\Omega)$

$$\left\| A_h^{-1}\phi \right\|_{L^\infty(\Omega)} \leq C \|\phi\|^{\frac{1}{2}}_{L^2(\Omega)} \left\| A_h^{-1}\phi \right\|^{\frac{1}{2}}_{H^1(\Omega)} + \left\| A_h^{-1}\phi \right\|_{H^1(\Omega)}. \tag{A.3}$$

Hence, it will be sufficient to take $\phi = A_h\chi$ to establish (A.2). To this scope, we decompose for $\phi \in U_h \cap H^1_*(\Omega)$

$$A_h^{-1}\phi = \mathcal{P}_{U_h} A^{-1}\phi + \left(A_h^{-1} - \mathcal{P}_{U_h} A^{-1} \right) \phi = I + II, \tag{A.4}$$

where $\mathcal{P}_{U_h}$ is the orthogonal L^2-projection onto U_h and where A denotes the negative Laplacian. Note that we define $A_h^{-1}\phi$ and $A^{-1}\phi$ uniquely by requiring them to be contained in $H^1_*(\Omega)$. To estimate the first term, we shall use the interpolation inequality

$$\|\chi\|_{L^\infty(\Omega)} \leq C \|\Delta\chi\|^{1/2}_{L^2(\Omega)} \|\chi\|^{1/2}_{H^1(\Omega)} + \|\chi\|_{H^1(\Omega)}. \tag{A.5}$$

By [11,21], we have in space-dimension $d=3$

$$\|\chi\|_{L^\infty(\Omega)} \leq C \left\|D^2\chi\right\|^{\frac{1}{2}}_{L^2(\Omega)} \|\chi\|^{\frac{1}{2}}_{L^6(\Omega)} + \|\chi\|_{L^6(\Omega)}.$$

https://doi.org/10.4208/cicp.scpde14.39s Published online by Cambridge University Press

By elliptic regularity theory, we infer

$$\left\|D^2\chi\right\|_{L^2(\Omega)} \leq C\|\Delta\chi\|_{L^2(\Omega)} + \|\chi\|_{L^6(\Omega)},$$

and by Sobolev imbedding, we may bound

$$\|\chi\|_{L^6(\Omega)} \leq \|\chi\|_{H^1(\Omega)},$$

which proves (A.5).

For the first term of (A.4), we combine (A.5) with the L^∞-stability of $\mathcal{P}_{U_h}$ (see [17]) and obtain

$$\begin{aligned}
\left\|\mathcal{P}_{U_h}A^{-1}\phi\right\|_{L^\infty(\Omega)} \leq& C\left\|A^{-1}\phi\right\|_{L^\infty(\Omega)} \\
\leq& C\|\phi\|^{\frac{1}{2}}_{L^2(\Omega)}\left\|A^{-1}\phi\right\|^{\frac{1}{2}}_{H^1(\Omega)} + \left\|A^{-1}\phi\right\|_{H^1(\Omega)} \\
\leq& C\|\phi\|^{\frac{1}{2}}_{L^2(\Omega)}\left\|A_h^{-1}\phi\right\|^{\frac{1}{2}}_{H^1(\Omega)} + C\|\phi\|^{\frac{1}{2}}_{L^2(\Omega)}\left\|\left(A_h^{-1}\mathcal{P}_{U_h} - A^{-1}\right)\phi\right\|^{\frac{1}{2}}_{H^1(\Omega)} \\
&+ \left\|A_h^{-1}\phi\right\|_{H^1(\Omega)} + \left\|\left(A_h^{-1}\mathcal{P}_{U_h} - A^{-1}\right)\phi\right\|_{H^1(\Omega)}. \qquad \text{(A.6)}
\end{aligned}$$

Let us collect some more inequalities. Testing (A.1) by ϕ and using the inverse inequality

$$\|\phi\|_{H^1(\Omega)} \leq \frac{C}{h}\|\phi\|_{L^2(\Omega)}, \qquad \text{(A.7)}$$

for a proof see [4], we get

$$\begin{aligned}
\|\phi\|^2_{L^2(\Omega)} =& \int_\Omega \nabla A_h^{-1}\phi\cdot\nabla\phi \\
\leq& \left\|A_h^{-1}\phi\right\|_{H^1(\Omega)}\|\phi\|_{H^1(\Omega)} \\
\leq& \frac{C}{h}\left\|A_h^{-1}\phi\right\|_{H^1(\Omega)}\|\phi\|_{L^2(\Omega)}.
\end{aligned}$$

Hence, $\|\phi\|_{L^2(\Omega)} \leq \frac{C}{h}\|A_h^{-1}\phi\|_{H^1(\Omega)}$ and therefore

$$\|A_h\phi\|_{L^2(\Omega)} \leq \frac{C}{h}\|\phi\|_{H^1(\Omega)}. \qquad \text{(A.8)}$$

As a consequence,

$$\|A_h\|_{H^1(\Omega)\to L^2(\Omega)} \leq \frac{C}{h}.$$

By standard error estimates (cf. [6]) and (A.8), we find

$$\begin{aligned}
\left\|A_h^{-1}\mathcal{P}_{U_h}\phi - A^{-1}\phi\right\|_{H^1(\Omega)} \leq& Ch\left\|A^{-1}\phi\right\|_{H^2(\Omega)} \\
\leq& Ch\|\phi\|_{L^2(\Omega)} = Ch\left\|A_hA_h^{-1}\phi\right\|_{L^2(\Omega)} \\
\leq& Ch\|A_h\|_{H^1(\Omega)\to L^2(\Omega)}\left\|A_h^{-1}\phi\right\|_{H^1(\Omega)} \leq C\left\|A_h^{-1}\phi\right\|_{H^1(\Omega)}, \qquad \text{(A.9)}
\end{aligned}$$

https://doi.org/10.4208/cicp.scpde14.39s Published online by Cambridge University Press

where we used elliptic regularity and the zero mean value of ϕ in the second step. Together with (A.6), this gives the desired estimate for the first term in (A.4). In addition, the last term in (A.6) is controlled in the desired way.

To control II in (A.4), we use the discrete Sobolev inequality

$$\|\phi\|_{L^\infty(\Omega)} \leq Ch^{-\frac{1}{2}} \|\phi\|_{H^1(\Omega)}$$

(see [10, p. 77]) to get

$$\begin{aligned}
\left\| \left(A_h^{-1} - \mathcal{P}_{U_h} A^{-1} \right) \phi \right\|_{L^\infty(\Omega)} &\leq Ch^{-\frac{1}{2}} \left\| \mathcal{P}_{U_h} \left(A_h^{-1} \mathcal{P}_{U_h} - A^{-1} \right) \phi \right\|_{H^1(\Omega)} \\
&\leq Ch^{-\frac{1}{2}} \left\| A^{-1}\phi \right\|_{H^2(\Omega)}^{\frac{1}{2}} h^{\frac{1}{2}} \left\| \mathcal{P}_{U_h} \left(A_h^{-1} \mathcal{P}_{U_h} - A^{-1} \right) \phi \right\|_{H^1(\Omega)}^{\frac{1}{2}} \\
&\leq C \|\phi\|_{L^2(\Omega)}^{\frac{1}{2}} \left\| A_h^{-1}\phi \right\|_{H^1(\Omega)}^{\frac{1}{2}}.
\end{aligned}$$

Note that the H^1-error estimate for linear finite elements, elliptic regularity theory, and (A.9) entered the last steps in this derivation. □

Corollary A.1. *Let $\Delta_h : U_h \to U_h \cap H^1_*(\Omega)$ be the discrete Laplacian as defined in* (2.10)*. Then there is a positive constant C, such that*

$$\|\chi\|_{L^\infty(\Omega)} \leq C \|\Delta_h \chi\|_{L^2(\Omega)}^{\frac{1}{2}} \|\chi\|_{H^1(\Omega)}^{\frac{1}{2}} + \|\chi\|_{H^1(\Omega)}$$

for all $\chi \in U_h$.

Proof. By using the h-independent equivalence of L^2-scalar product and lumped masses scalar product (see (2.2)), we compute

$$\|A_h \chi\|_{L^2(\Omega)}^2 = \int_\Omega \nabla \chi \cdot \nabla A_h \chi = -(\Delta_h \chi, A_h \chi)_h \leq C \|\Delta_h \chi\|_h \|A_h \chi\|_{L^2(\Omega)}.$$

This implies

$$\|A_h \chi\|_{L^2(\Omega)} \leq \tilde{C} \|\Delta_h \chi\|_{L^2(\Omega)}.$$

This completes the proof. □

Acknowledgments

This research has been supported by Deutsche Forschungsgemeinschaft (German Science Foundation) through the Priority Programme 1506 "Transport processes at fluidic interfaces" and by Ministerio de Economía y Competividad (Spain) through the project MTM2012-32325. Hubertus Grillmeier made major contributions to the implementation of the axial-symmetric version of the scheme in 3D. Parts of this work have been written while the first author visited Universidad de Sevilla, other parts have been written while the second author visited University of Erlangen-Nürnberg. The hospitality of these institutions is gratefully acknowledged.

https://doi.org/10.4208/cicp.scpde14.39s Published online by Cambridge University Press

References

[1] H. Abels, H. Garcke, and G. Grün, *Thermodynamically consistent, frame indifferent diffuse interface models for incompressible two-phase flows with different densities*, Mathematical Models and Methods in Applied Sciences **22** (2012), no. 3, 1150013.

[2] S. Aland, S. Boden, A. Hahn, F. Klingbeil, M. Weismann, and S. Weller, *Quantitative comparison of Taylor flow simulations based on sharp-interface and diffuse-interface models*, International Journal for Numerical Methods in Fluids **73** (2013), no. 4, 344–361.

[3] F. Armero and J.C. Simo, *Formulation of a new class of fractional-step methods for the incompressible mhd equations that retains the long-term dissipativity of the continuum dynamical system*, Fields Institute Communications, **10** (1996), 1-24.

[4] S. C. Brenner and L. R. Scott, *The Mathematical Theory of Finite Element Methods*, Springer, 2002.

[5] E. Campillo-Funollet, G. Grün, and F. Klingbeil, *On modeling and simulation of electrokinetic phenomena in two-phase flow with general mass densities*, SIAM Journal on Applied Mathematics **72** (2012), no. 6, 1899–1925.

[6] P. G. Ciarlet, *The finite element method for elliptic problems*, Classics in applied Mathematics, vol. 40, Society for Industrial and Applied Mathematics, Philadelphia, US-PA, 2002.

[7] H. Ding, P. D. M. Spelt, and C. Shu, *Diffuse interface model for incompressible two-phase flows with large density ratios*, Journal of Computational Physics **226** (2007), 2078–2095.

[8] C. R. Dohrmann and P. B. Bochev, *A stabilized finite element method for the Stokes problem based on polynomial pressure projections*, International Journal for Numerical Methods in Fluids **46** (2004), 183–201.

[9] C. Eck, M. A. Fontelos, G. Grün, F. Klingbeil, and O. Vantzos, *On a phase-field model for electrowetting*, Interfaces and Free Boundaries **11** (2009), 259–290.

[10] A. Ern and J. Guermond, *Theory and practice of finite elements*, Springer Series in Applied Mathematical Sciences, vol. 159, Springer, New York, US-NY, 2004.

[11] E. Gagliardo, *Ulteriori propriet di alcune classi di funzioni in più variabili.*, Ricerche di Matematica **8** (1959), 24–51.

[12] G. Grün, *On convergent schemes for diffuse interface models for two-phase flow of incompressible fluids with general mass densities*, SIAM Journal on Numerical Analysis **51** (2013), no. 6, 3036–3061.

[13] G. Grün and F. Klingbeil, *Two-phase flow with mass density contrast: Stable schemes for a thermodynamic consistent and frame-indifferent diffuse-interface model*, Journal of Computational Physics **257, Part A** (2014), 708–725.

[14] F. Guillén-González and G. Tierra, *Splitting schemes for a Navier–Stokes–Cahn–Hilliard model for two fluids with different densities*, Journal of Computational Mathematics **32** (2014), no. 6, 643–664.

[15] C. Kahle H. Garcke, M. Hinze, *A stable and linear time discretization for a thermodynamically consistent model for two-phase incompressible flow*, Hamburger Beiträge zur Angewandte Mathematik (2014).

[16] A. Hansbo, *Strong stability and non-smooth data error estimates for discretizations of linear parabolic problems*, BIT **42** (2002), no. 2, 351–379.

[17] Jr. J. Douglas, T. Dupont, and L. Wahlbin, *The stability in l^q of the l^2-projection into finite element function spaces*, Numerische Mathematik **23** (1975), 193–197.

[18] S. Minjeaud, *An unconditionally stable uncoupled scheme for a triphasic cahn–hilliard/navier-stokes model.*, Numerical Methods for PDE **29** (2013), no. 2, 584–618.

https://doi.org/10.4208/cicp.scpde14.39s Published online by Cambridge University Press

[19] L. Modica, *The gradient theory of phase transitions and the minimal interface criterion*, Archive for Rational Mechanics and Analysis **98** (1987), 123–142.
[20] L. Modica and S. Mortola, *Un esempio di γ-convergenza*, Bollettino dell'Unione Matematica Italiana **B 14** (1977), 285–299.
[21] L. Nirenberg, *On elliptic partial differential equations.*, Annali della Scuola Normale Superiore di Pisa **13** (1959), 115–162.
[22] T. Qian, X. Wang, and P. Sheng, *A variational approach to the moving contact line hydrodynamics*, Journal of Fluid Mechanics **564** (2006), 333–360.
[23] H. Werner and H. Arndt, *Gewöhnliche Differentialgleichungen*, Springer-Verlag, Berlin–Heidelberg, 1991.
[24] P. Yue, J. J. Feng, C. Liu, and J. Shen, *A diffuse-interface method for simulating two-phase flows of complex fluids*, Journal of Fluid Mechanics **515** (2004), 293–317.

https://doi.org/10.4208/cicp.scpde14.39s Published online by Cambridge University Press